Natural Resources Canada | Ressources naturelles Canada

GEOLOGICAL SURVEY OF CANADA
OPEN FILE 8869

Distributions of degraded and intact lithalsas, North Slave region, Northwest Territories

P.D. Morse and A.C.A Rudy

2022

Canada

GEOLOGICAL SURVEY OF CANADA
OPEN FILE 8869

Distributions of degraded and intact lithalsas, North Slave region, Northwest Territories

P.D. Morse[1] and A.C.A Rudy[2]

[1]Geological Survey of Canada, 601 Booth Street, Ottawa, Ontario
[2]Northwest Territories Geological Survey, 4601 52nd Avenue, Yellowknife, Northwest Territories

2022

Permanent link: https://doi.org/10.4095/329643

This publication is available for free download through GEOSCAN (https://geoscan.nrcan.gc.ca/).

Recommended citation

Morse, P.D. and Rudy, A.C.A., 2022. Distributions of degraded and intact lithalsas, North Slave region, Northwest Territories; Geological Survey of Canada, Open File 8869, 1 .zip file. https://doi.org/10.4095/329643

ABSTRACT
The main objective of this report is to provide an inventory of current (intact or degrading) and old (completely degraded) lithalsas in a representative study area of the southern North Slave region between Behchoko and Yellowknife in the Northwest Territories. A lithalsa is an ice-rich mound of permafrost that causes the soil to settle downward and water to pond if the ice core thaws (thermokarst pond). Lithalsas, widespread in this region, are therefore very sensitive to thawing. This inventory should help to better understand current and future permafrost conditions, and is based directly on the GSC's Open File 7255, which provides an inventory of many lithalsas in the region, as well as on the GSC's Open File 8205, which provides an inventory of thermokarst pond development between 1945 and 2005 in the same study area. Using high-resolution satellite images, we completed the inventory of 475 intact lithalsas in the study area. Then, by combining our field observations of surface geomorphology of degrading lithalsas with recognizable geomorphic patterns in the same satellite imagery, we developed criteria to identify and map them and we developed an inventory of 556 completely degraded lithalsas. The inventories and databases are prepared for assessment of the relations between elevation, surface geology and distribution of lithalsas, and the trajectory of thermokarst development in the region. The inventories included with this report can be used directly in a Geographic Information System (GIS).

DISCLAIMER

Her Majesty the Queen in right of Canada, as represented by the Minister of Natural Resources ("Canada"), does not warrant or guarantee the accuracy or completeness of the information ("Data") and does not assume any responsibility or liability with respect to any damage or loss arising from the use or interpretation of the Data.

The Data are intended to convey regional trends and should be used as a guide only. The Data should not be used for design or construction at any specific location, nor are the Data to be used as a replacement for the types of site-specific geotechnical investigations.

TABLE OF CONTENTS

LIST OF FIGURES

Page

LIST OF TABLES

Page

1 INTRODUCTION

Permafrost terrain, the foundation of many northern landscapes, is the environmental setting for the flora and fauna relied upon by northern societies, it supports the built environment required for northern development and prosperity, and its presence affects interactions between surface and ground water resources. Many northern localities are exhibiting signs of permafrost thaw, which is significant as the associated effects are expected to directly impact northern ecosystems and infrastructure. In order to develop adequate adaptation strategies and measures, it is essential to characterize and quantify thaw sensitive terrain.

Permafrost, largely a function of climate conditions, can thaw due to climate warming or to changes to local surface conditions such as forest fire (e.g., Zhang et al. 2015). Permafrost often contains ice, and thaw of ice rich permafrost often leads to ground settlement, surface water ponding in the resulting depression, and development of characteristic landforms, collectively termed "thermokarst". In the southern North Slave region (Figure 1a) permafrost is in thermal disequilibrium with climate and is warming (Morse et al. 2015; Wolfe et al. 2015), and wildfires are relatively common (ENR 2015). Ice-rich permafrost is associated with the distribution of fine-grained sediments (Morse et al. 2015; Gaanderse et al. 2018; Paul et al. 2021), as is widespread thermokarst (Figure 2), which is often a direct result of the degradation of ice-cored permafrost mounds called "lithalsas" (Figures 1b and 1c) (Morse et al. 2017). Lithalsas, which are numerous in this region (Figure 2) (Stevens et al. 2012a), are perennial frost mounds with cores of segregated ice in mineral deposits and little to no surface organic cover (Harris 1993). They formed here during the Holocene with permafrost aggradation as lake levels receded due to isostatic rebound (Wolfe and Morse 2017, Gaanderse et al. 2018). Many contemporary lithalsas are in a state of degradation and exhibit a distinct geomorphic, rampart-thermokarst pond pattern (Figure 1c) that may be used to map the former locations of lithalsas, which is a useful indication of thaw sensitive terrain and provides further insights on landscape evolution in this region.

This report builds on earlier mapping in this region of lithalsas (Stevens et al. 2012a) and of thermokarst ponds that developed between 1945 and 2005 (Morse et al. 2017). Using the study area from Morse et al (2017), which is representative of the region, the research objectives were to: (i) extend the existing inventory of lithalsa locations across the elevational gradient that constrains the regional landscape history, and (ii) use the rampart-thermokarst pond pattern to identify former lithalsa locations and map their areas. Whereas Morse et al. (2019) summarized the location data and developed these into a conceptual model for lithalsa degradation, the primary purpose of this Open File is to present these inventories of both location and area in detail with respect to elevation and surficial geology, and make them publicly available.

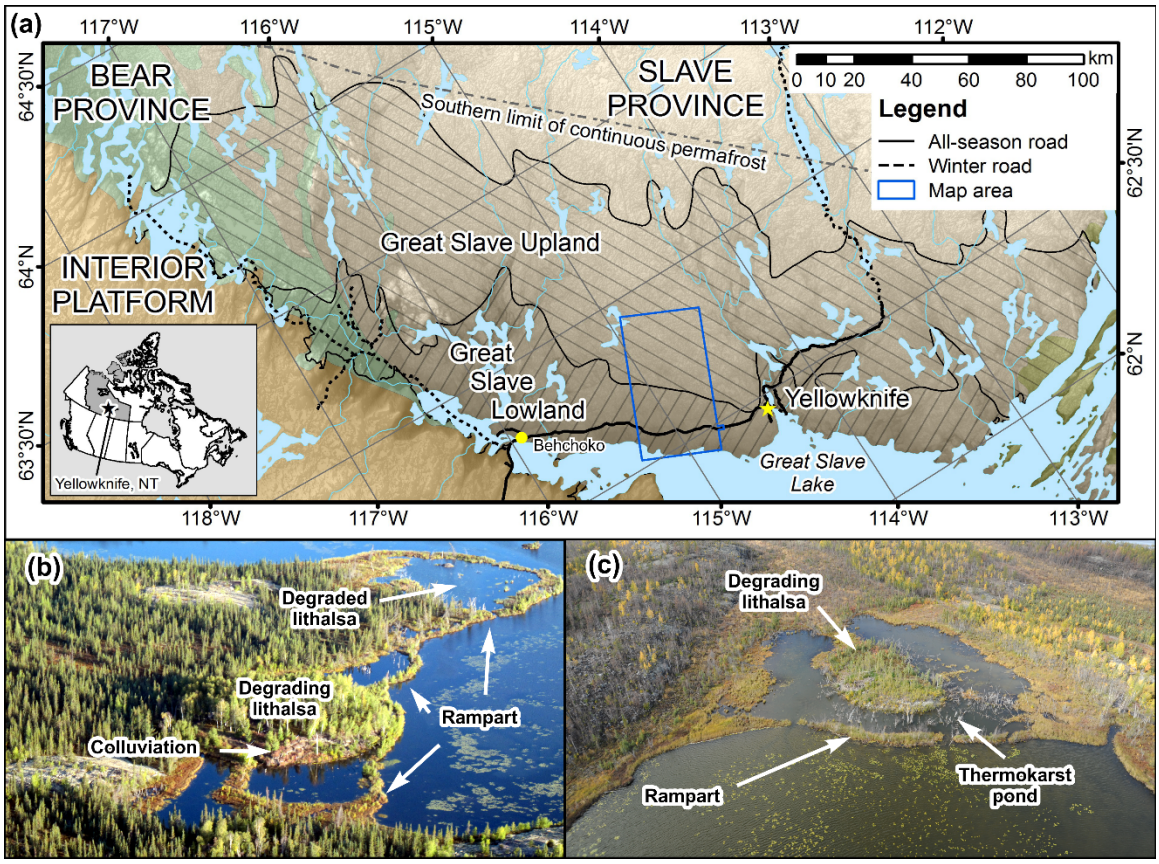

Figure 1. (a) Great Slave Upland and Lowland regions, southern subarctic Canadian Shield. The blue rectangle outlines the study area. (b) Example of a complex of degrading lithalsas near the modern shoreline of Great Slave Lake. Photograph by C.W. Stevens. NRCan photo 2020-935. (c) Example of a lithalsa at higher elevation in the Great Slave Lowland with dead trees standing in the thermokarst pond. Photograph by P.D. Morse. NRCan Photo 2020-936.

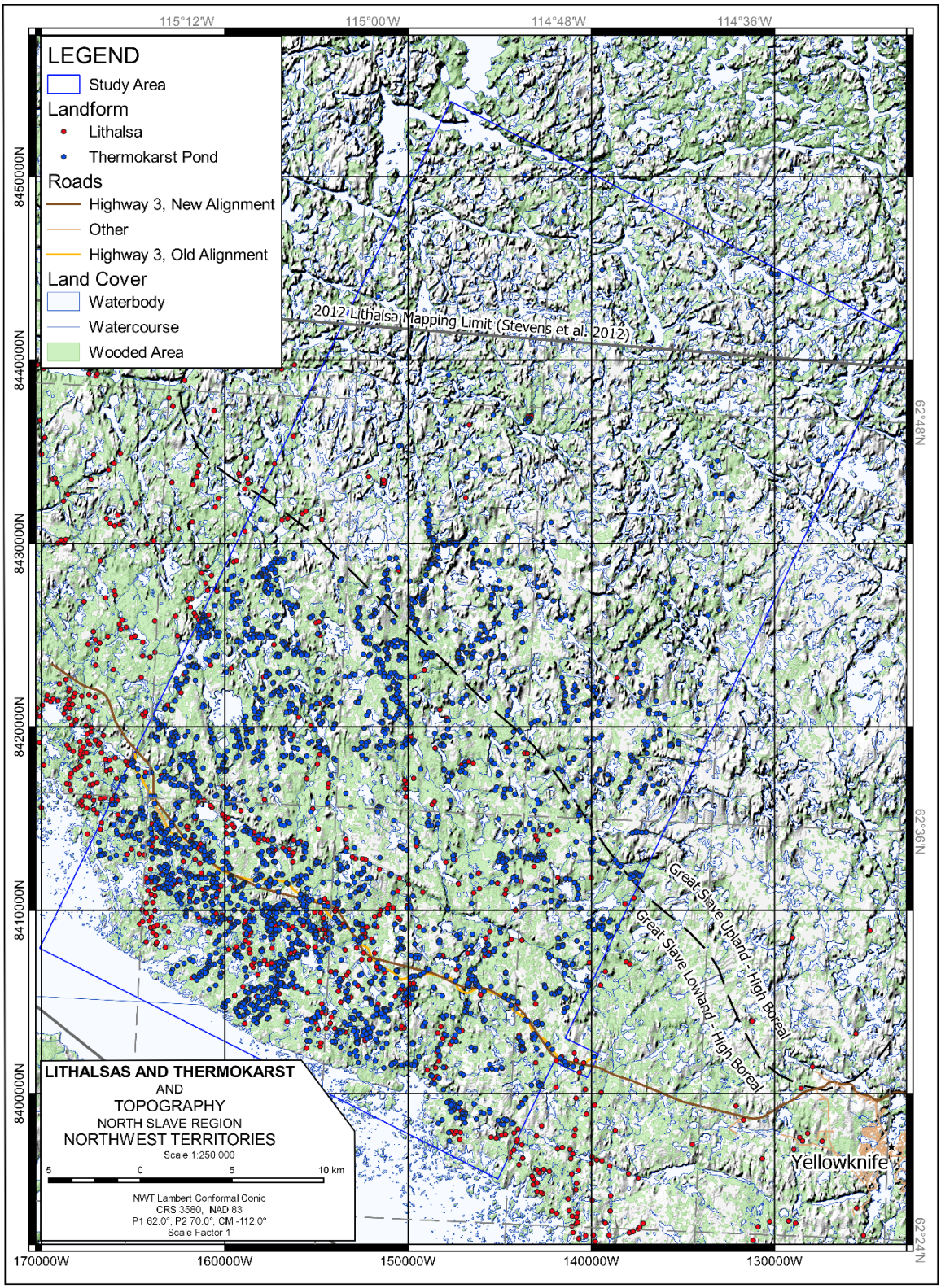

Figure 2. Distribution of mapped lithalsas (Stevens et al. 2012a) and thermokarst ponding (1945-2005) (Morse et al. 2017), North Slave Region, NT.

Importantly, the data presented here are updated with respect to elevation according to a new, very high-resolution composite digital elevation model (DEM), derived from High Resolution Digital Elevation Model (HRDEM) (NRCan 2019) and Advanced Land Observing Satellite Global Digital Surface Model "ALOS World 3D - 30m" (ALOS AW3D30) (JAXA 2020), the use of which eliminates gross elevation errors introduced by artifacts present in the Canadian Digital Elevation Model (CDEM) that was used earlier (e.g., Stevens et al. 2012a, Morse et al. 2019). The development of the composite DEM used in the present analysis, along with the various elevation issues associated with alternative DEMs, is presented in Appendix A.

2 BACKGROUND

The study region is in the southern Tłicho Region, subarctic Northwest Territories, north of Great Slave Lake (Figure 1a). Located in the southern Slave Geological province of the Canadian Shield, it is a low elevation Precambrian, granitic bedrock plain. The plain features an array of surficial materials that were deposited as a direct result of glaciation and deglaciation which began in this region about 12 700 cal BP with retreat of the Laurentide Ice Sheet (Wolfe et al. 2017). Glacial Lake McConnell was subsequently established for about 3 400 years (Wolfe et al. 2017), after which lake levels began to decline gradually, continuing down over the last 8000 years at a rate of about 5 mm a^{-1} to the present elevation of Great Slave Lake (Wolfe and Morse 2017).

With terrestrial emergence, surficial deposits in the region were progressively reworked by shoreline processes, which was accompanied by sediment deposition in deeper basins. As a result of this landscape history the study area contains two ecoregions, Great Slave Upland (GSU) and Great Slave Lowland (GSL) (Figure 1a; Ecosystem Classification Group 2018). GSU is dominated by bedrock with thin discontinuous deposits of wave-eroded tills, and glaciolacustrine sediments and glaciofluvial materials occur between bedrock outcrops. GSL, lower in elevation, was once part of the depositional basin, and nearly 70% is covered by glaciolacustrine and nearshore lacustrine deposits (Wolfe et al. 2014).

The regional permafrost distribution, which is discontinuous (Heginbottom et al. 1995; Morse et al. 2015), is related to the Holocene lake-level recession (Wolfe and Morse 2017). Permafrost, which aggraded following terrestrial emergence (Wolfe and Morse 2017), occurs in fine-grained sediments covered by peatlands or forests (Morse et al. 2015), but is typically not present beneath bedrock outcrops or in coarse-grained, unconsolidated sediments (Brown 1973). Where present, permafrost is up to 50 m thick (Brown 1973), and occurs beneath a thick active layer (0.30 to 1.30 m) (Morse et al. 2015). Ground ice development accompanied permafrost aggradation (Wolfe and Morse 2017), as indicated by high near-surface ground ice contents in fine-grained sediments

(Morse et al. 2015, Gaanderse et al. 2018; Paul et al 2021), and by the formation of lithalsas throughout the GSL and GSU (Figure 2) (Wolfe at al. 2014).

Climate and vegetation distribution in the region have changed substantially since deglaciation. Climate was cooler than present before about 6000 cal BP and GSU vegetation consisted of tundra, shub tundra, and taiga (Huang et al. 2004). Then climate warmed until about 3500 cal BP and treeline advanced northward (Moser and MacDonald 1990; MacDonald et al. 1993). After a period of relative stability, climate subsequently cooled, beginning around 3000 cal BP, and treeline retreated to its present location (Huang et al. 2004). Since the meteorological record began in the 1940s, annual mean air temperatures in Yellowknife have increased (Riseborough et al. 2013). Indeed, between the 1971-2000 and 1981-2010 climate normal, mean annual air temperature at Yellowknife Airport has increased 0.3 °C (Environment Canada 2020). This regional air temperature trend has produced warm, disequilibrium permafrost thermal conditions (mean annual ground temperatures range from -1.4 °C to 0.0 °C) (Morse et al. 2015; Wolfe et al. 2015), and if the climate warming trend continues, Zhang et al. (2014) predict that regional permafrost extent will reduce from 52.0 % in the 2000s to 2.5% in the 2090s.

Presently, the landscape is a mosaic of numerous waterbodies, rocks, forests, and peatlands, and permafrost throughout the fine-grained deposits of GSL and GSU exhibits signs of degradation as near-surface ground ice thaw has produced thermokarst ponds (Figure 2) that are frequently associated with degrading lithalsas (Figures 1b and 1c) (Morse et al. 2017, 2019). Lithalsas in this region are widespread (Figure 2) (Wolfe et al. 2014), in association with fine-grained glaciolacustrine and alluvial deposits (Wolfe et al. 2014, Wolfe and Morse 2017, Gaanderse et al. 2018), and develop adjacent to water bodies that likely supply the water for ice segregation (Gaanderse et al. 2018). Varying in shape from round, to crescentic, to ridge-like, these lithalsas have up to 8 m of relief and can be several hundred metres in length (Wolfe et al. 2014). In this region, lithalsas are visually distinct from the surrounding black spruce forest (*Picea mariana*), due to their contrasting forest canopy of white birch (*Betula papyrifera*) and white spruce (*Picea glauca*) (Wolfe et al. 2014, Morse et al. 2015, Paul et al. 2021). The contrast is likely due to improved drainage and deeper active layer on lithalsas which facilitate their growth. Degrading lithalsas are characterized by a thermokarst pond that develops as the lithalsa collapses, which is retained by a rampart (rim-ridge) that demarks the maximum extent (Figures 1b and 1c), and with a completely degraded lithalsa only the rampart and pond may remain (Figure 1b) (e.g., Dionne 1978, Pissart 2002, Calmels et al. 2008). The thermokarst pond often exhibits standing dead white birch or white spruce trees, which contrasts with the adjacent water body on the other side of the rampart (Figure 1c).

3 STUDY AREA

The study area (~1430 km^2), established by Morse et al. (2017) to test the hypothesized relation between thermokarst, surficial geology, and elevation, is located approximately 20 km northeast of Yellowknife and oriented along the regional topographic-geological history gradient (Figure 1). Elevations within the study area (see Appendix A) range from 154 to 274 m a.s.l., and generally increase in a north-easterly direction from the shoreline of Great Slave Lake (Figure 3a). The surficial geology of the study area mapped by Stevens et al. (2012b) is dominated by bedrock outcrop (R) and glaciolacustrine deposits (GL), with comparatively sparse glaciofluvial (GF) and organic (O) deposits (Figure 3b). The increased extent of GL at lower elevations is a direct function of the transient landscape history, and the northern limit of its extensive distribution is approximated by the boundary between GSL and GSU which has an average elevation of 200 m a.s.l.

4 METHODS

4.1 Image Data

This study uses very high-resolution satellite images satellite images (0.6-m resolution DigitalGlobe^{TM} data acquired in 2005 and displayed in GoogleEarth^{TM}) for feature mapping. We use the image data to update the lithalsa inventory of Stevens et al. (2012a) so that it is complete within our study area, and to create the new inventory of completely degraded lithalsas.

4.2 Digital Elevation Data (DEM)

Elevation data used in the analysis are a composite of ALOS AW3D30 (JAXA 2020) and HRDEM (NRCan 2019) datasets (Figure 3). Appendix A details the creation of the composite DEM. which was used to assign elevations to newly digitized features and to update elevations of previously mapped lithalsas (Stevens et al. 2012a) and thermokarst ponds (Morse et al. 2017).

4.3 Digitization

Degrading lithalsas often exhibit tell-tale geomorphic elements that include the presence of a visible rampart that is often accompanied by standing dead vegetation in the adjacent thermokarst pond (e.g., Figures1a and 1b). We mapped degraded lithalsas according to these diagnostic criteria. As the thermokarst ponds mapped by Morse et al. (2017) account for degradation since 1945, the degraded lithalsas that we mapped represent those that had decayed before 1945. Using the criteria established in Stevens et al. (2012a), and their lithalsa data as training points, we identified and mapped lithalsas in our study area that were beyond the limit of their study area.

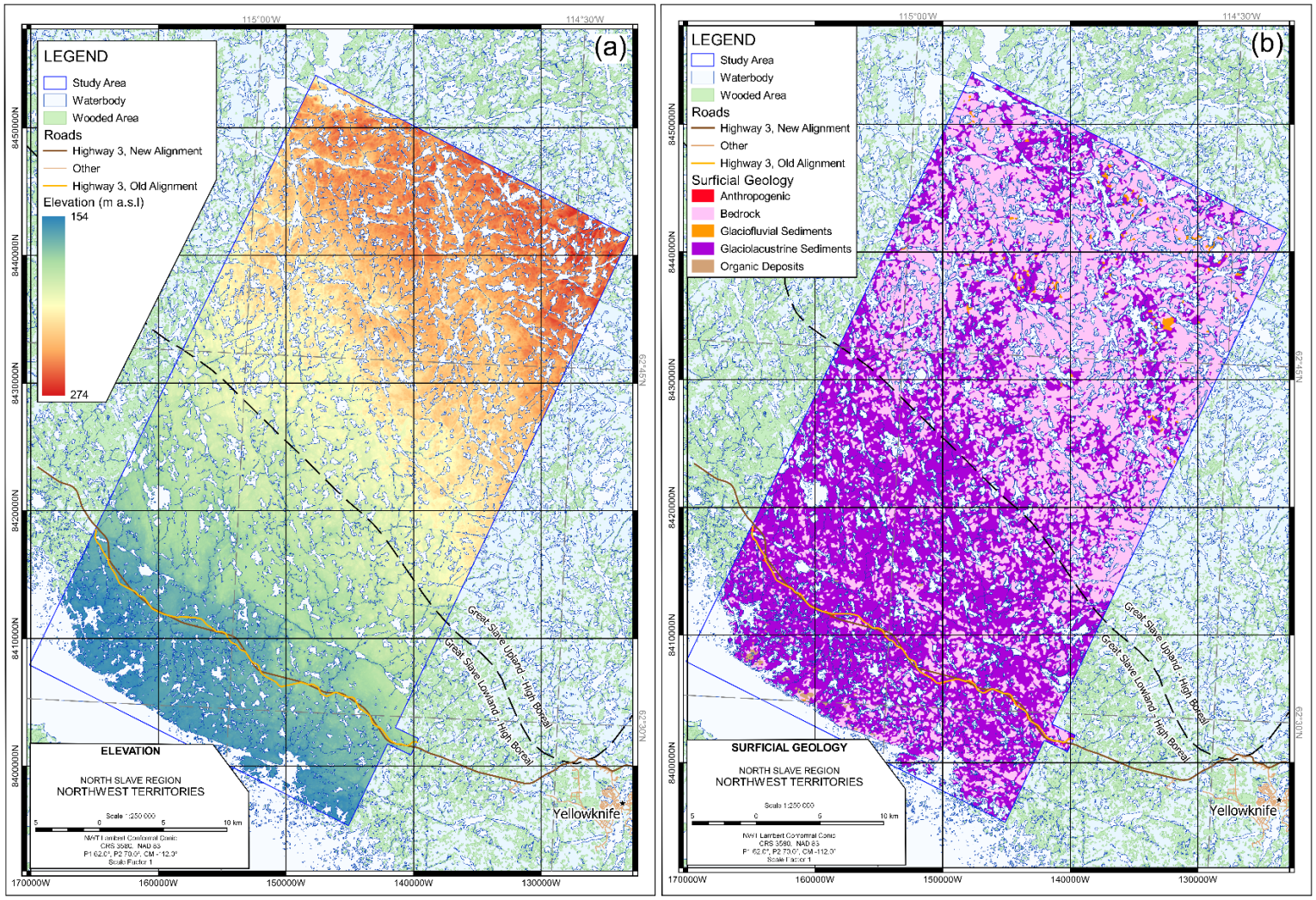

Figure 3. (a) Elevation (source: Appendix A), and (b) surficial geology (source: Stevens et al. 2012b) within the study area.

All feature digitization was carried out using Google Earth™ at a scale of about 1:2500. The extent of any degraded lithalsa evident in the satellite image was manually digitized using the "Polygon" tool, and the location of any lithalsa was digitized using the "Point" tool. The margin of error for an individual lithalsa area is likely on the order of ±50 m^2. Digitized polygons and points were exported from Google Earth™ to a Geographic Information System for spatial analysis.

4.4 Processing and Analysis

All digitized degraded lithalsas were combined into one file, and newly mapped lithalsas were combined with points extracted for the study area from those mapped by Stevens et al. (2012a). As with earlier analysis of thermokarst ponds (Morse et al. 2017), we generated a point file of degraded lithalsa centroids. We then carried out an overlay analysis in the GIS to assign elevation and surficial geology values to the lithalsa and degraded lithalsa point data. The attributes of the degraded lithalsa centroids were then passed on to the parent polygon. Knowing that the elevations for thermokarst ponds reported in Morse et al. (2017) are affected by comparatively gross, systematic errors in the CDEM versus the new composite DEM for the study area, we also updated the attributes of the thermokarst pond data with new elevation values. Tables 1 to 3 summarize the attributes of the point and polygon features. Once all attributes were assigned to the points and polygons, we queried them to examine geomorphic feature distributions with respect to elevation and surficial geology. We used a normalized difference expressed as a percentage to summarize the difference in landform counts for a given elevation range according to:

$$\frac{(a-b)}{(a+b)} \times 100 \qquad [1]$$

where a and b are the counts (n) of intact and degraded lithalsas, respectively.

4.5 Limitations

The main objective of this research is a first order estimation of the extent of degraded lithalsas in the study area. As such, the digitizing process involved expert decision that, though dependent on personal interpretation, was deemed sufficient to fulfill the objectives at hand. A quality control assessment was carried out by a second expert who corrected any errors. However, our mapping approach implies that we can only map features where the rampart is obvious, and therefore we likely exclude locations where a smaller lithalsa may have existed.

Regarding feature attribute extraction from surficial geology or elevation, we recognize the potential for the centroid to fall within a surficial geology polygon or on an elevation

Table 1. Summary of all point attributes in of8869_points.shp.

Attribute name	Attribute description	Type	Values
OID	Unique object identification number	Integer	1 to 4025
Type	Feature type	String	Lithalsa; Degraded Lithalsa; Thermokarst pond;
Elevation	Elevation above mean sea level (m)	Integer	154 to 252
SurfGeol	Simplified surficial geology type	String	GF = Glaciofluvial; GL = Glaciolacustrine; H = Anthropogenic; O = Organic; R = Rock; W = Water

Table 2. Summary of degraded lithalsa polygon attributes in of8869_dl_polys.shp.

Attribute name	Attribute description	Type	Values
OID	Unique object identification number	Integer	1 to 556
Elevation	Elevation above mean sea level (m)	Integer	156 to 249
SurfGeol	Simplified surficial geology type	String	GF = Glaciofluvial; GL = Glaciolacustrine; H = Anthropogenic; O = Organic; R = Rock; W = Water
Area	Polygon area (m^2)	Real	33 to 19327
Perimeter	Polygon perimeter (m)	Real	26 to 861

Table 3. Summary of thermokarst pond polygon attributes in of8869_tp_polys.shp.

Attribute name	Attribute description	Type	Values
OID	Unique object identification number	Integer	1 to 2994
Name	Unique pond name	String	*e.g.*, "Pond035"
XCentroid	Longitude of polygon centroid (decimal degrees)	Real	*e.g.*, -115.04013374500
YCentroid	Latitude of polygon centroid (decimal degrees)	Real	*e.g.*, 62.54727621600
Elevation	Elevation above mean sea level (m)	Integer	156 to 249
SurfGeol	Simplified surficial geology type	String	GF = Glaciofluvial; GL = Glaciolacustrine; H = Anthropogenic; O = Organic; R = Rock; W = Water
Area	Polygon area (m^2)	Real	11 to 43115
Perimeter	Polygon perimeter (m)	Real	17 to 2754

that is different from the surficial geology unit overlain by the majority of the polygon. Consequently, there may be some error associated with the method, but this is likely minimal due to the generally homogeneous surficial geology and elevation data at the scale of the mapping.

Finally, whereas features are digitized on the Google Earth™ image base, some localized georeferencing problems may occur in relation to the position of the imagery shown, but these individual errors are not considered significant as the results are considered in aggregate.

5 RESULTS AND DISCUSSION

5.1 Inventory of Degraded and Intact Lithalsas

Within the study area we mapped a total of 556 completely degraded lithalsas (0.54 km^2 pond area) (Figure 4). We also added 7 intact lithalsas to the 468 mapped by Stevens et al. (2012a) (Figure 5). These results indicate that there used to be more than twice as many lithalsas as occur today. Complimenting these counts are 2994 thermokarst ponds that developed between 1945 and 2005 (does not include ponds that developed from borrow pits used to build Old Highway 3; "Pond2066" in Morse et al. (2017) is outside the study area and was deleted) (Figure 2). As far as the authors are aware, this is the first inventory of degraded lithalsas compiled for any location, and the approach may be used to guide further investigations of thaw sensitive terrain in surrounding regions.

5.2 Degraded and Intact Llithalsa Distributions

The distributions of degraded and intact lithalsa within the study area are strongly related to elevation (Figures 6a and 7a,b). Nearly 96% of intact lithalsas and 64% of degraded lithalsas occur at less than 200 m a.s.l. (45 m above Great Slave Lake). Though both are common at elevations below 200 m a.s.l., there are generally greater number of intact lithalsas with the exception of high degraded lithalsa counts between 156 and 160 m a.s.l. (within 5 vertical m of Great Slave Lake level) (Figure 8a). Above 200 m a.s.l. the contribution to total counts in landforms from degraded lithalsa is consistently more than from intact lithalsas (Figure 8b). The total degraded lithalsa pond area of less than half a square kilometre is distributed relatively evenly across the elevation gradient, with the exception of a concentration below 165 m a.s.l. (Figure 9a). These results suggest that lithalsas were once more widespread throughout the study area up to an elevation of about 249 m a.s.l, but most lithalsas that developed above an elevation of about 200 m a.s.l have degraded (Figures 6a and 7).)

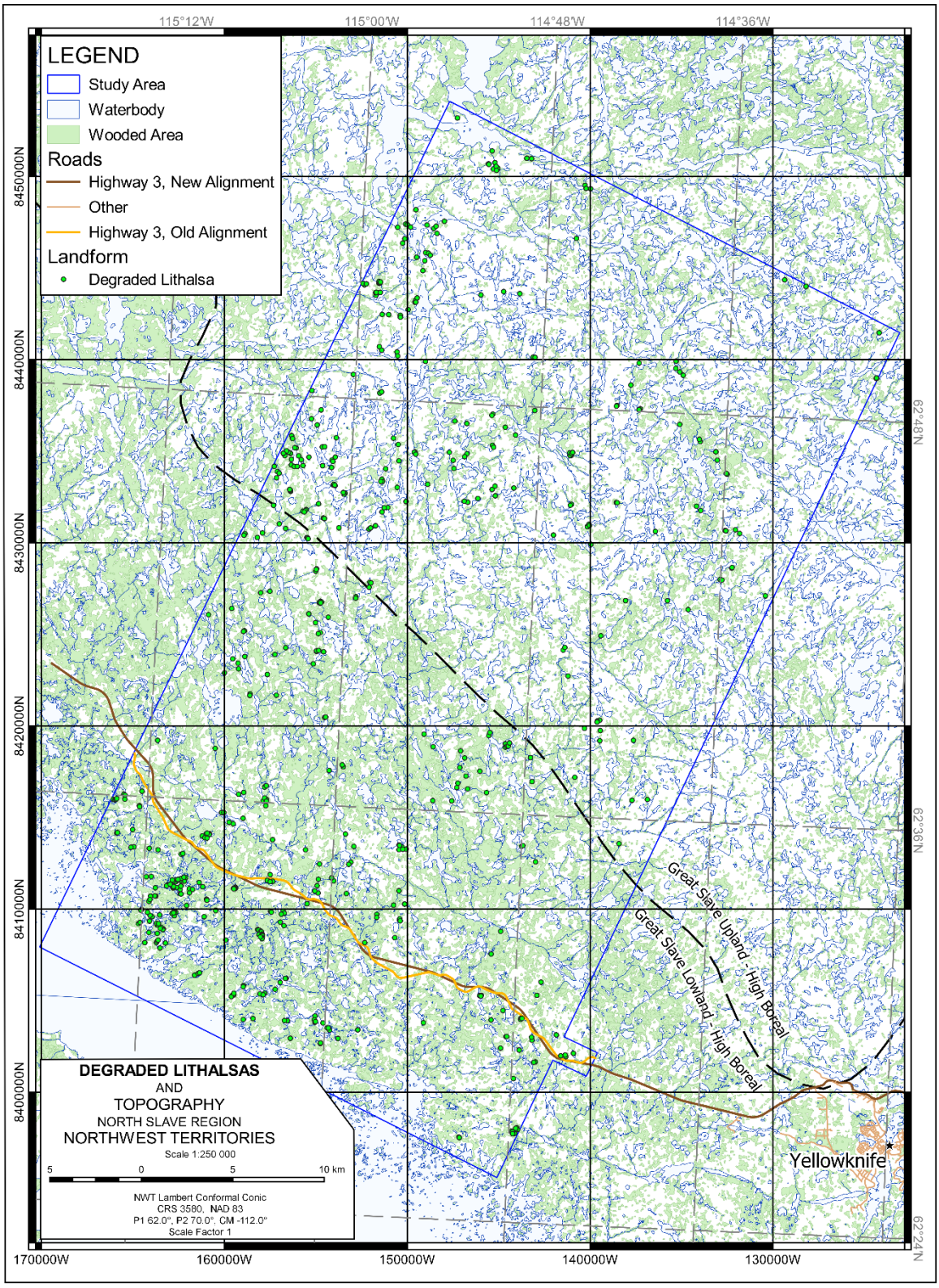

Figure 4. Distribution of degraded lithalsas in the North Slave region.

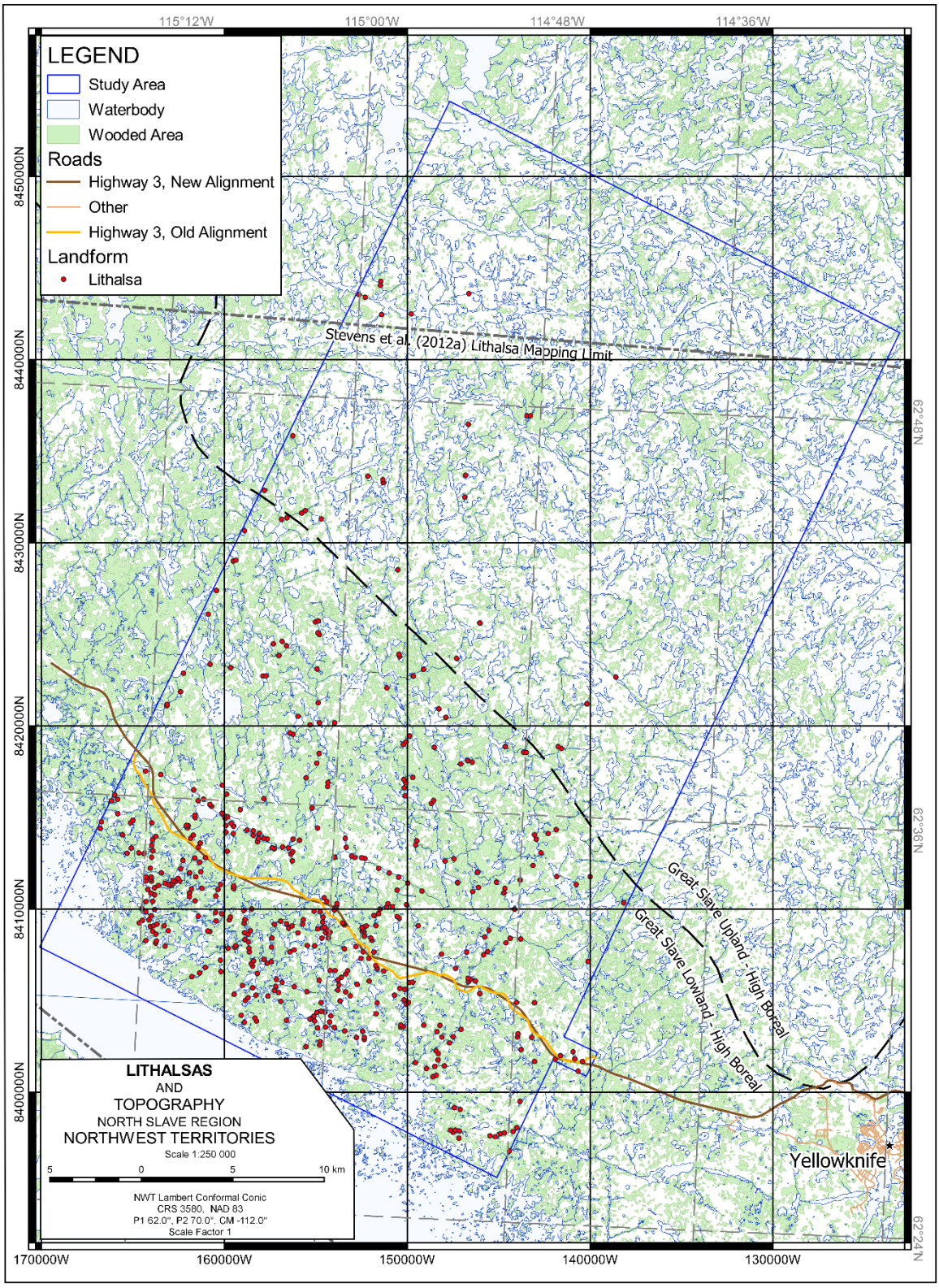

Figure 5. Distribution of lithalsas in the North Slave region. Note the lithalsa mapping limit of Stevens et al. (2012a).

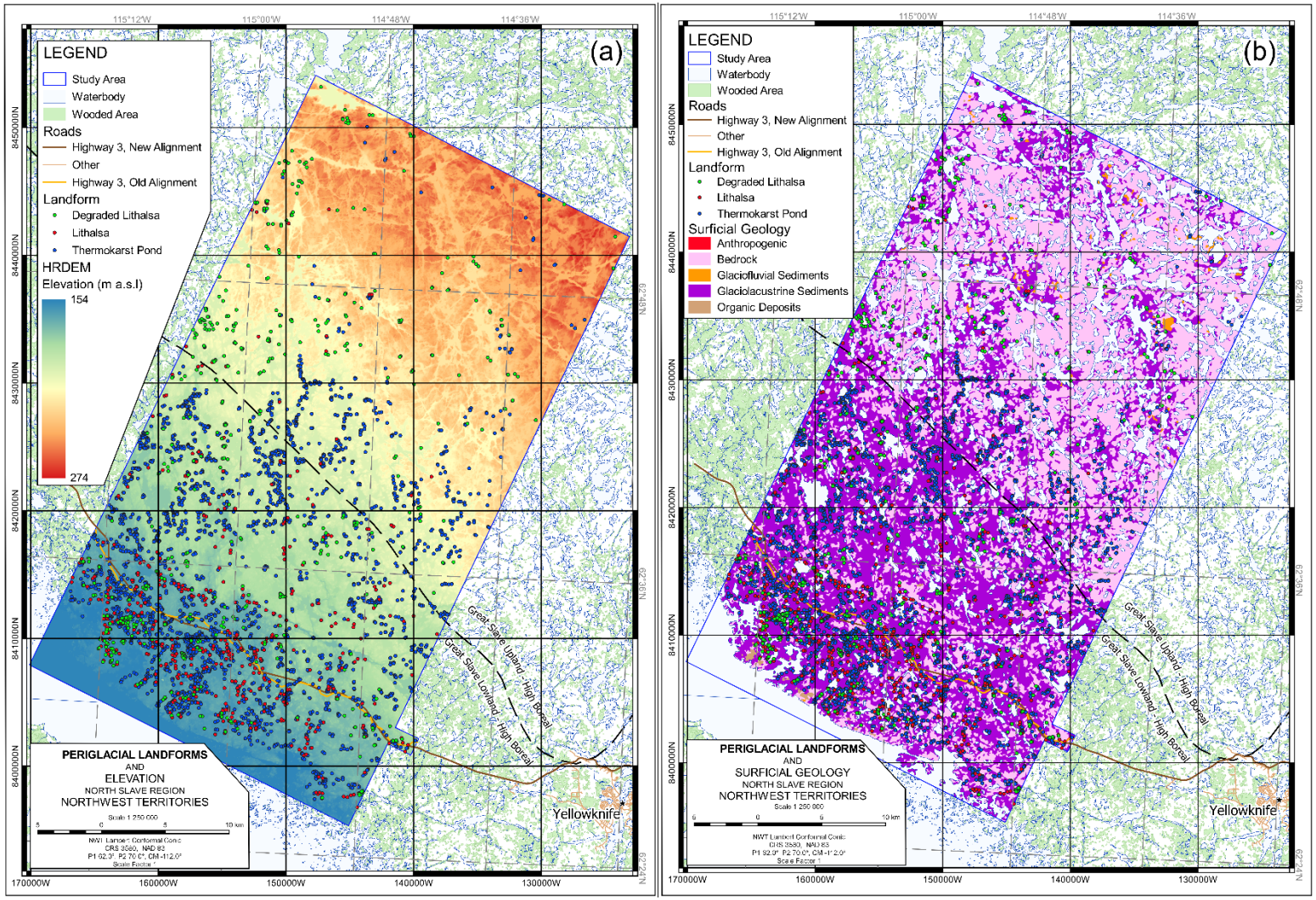

Figure 6. Distributions of degraded lithalsas, lithalsas, and thermokarst ponding with respect to (a) elevation and (b) surficial geology.

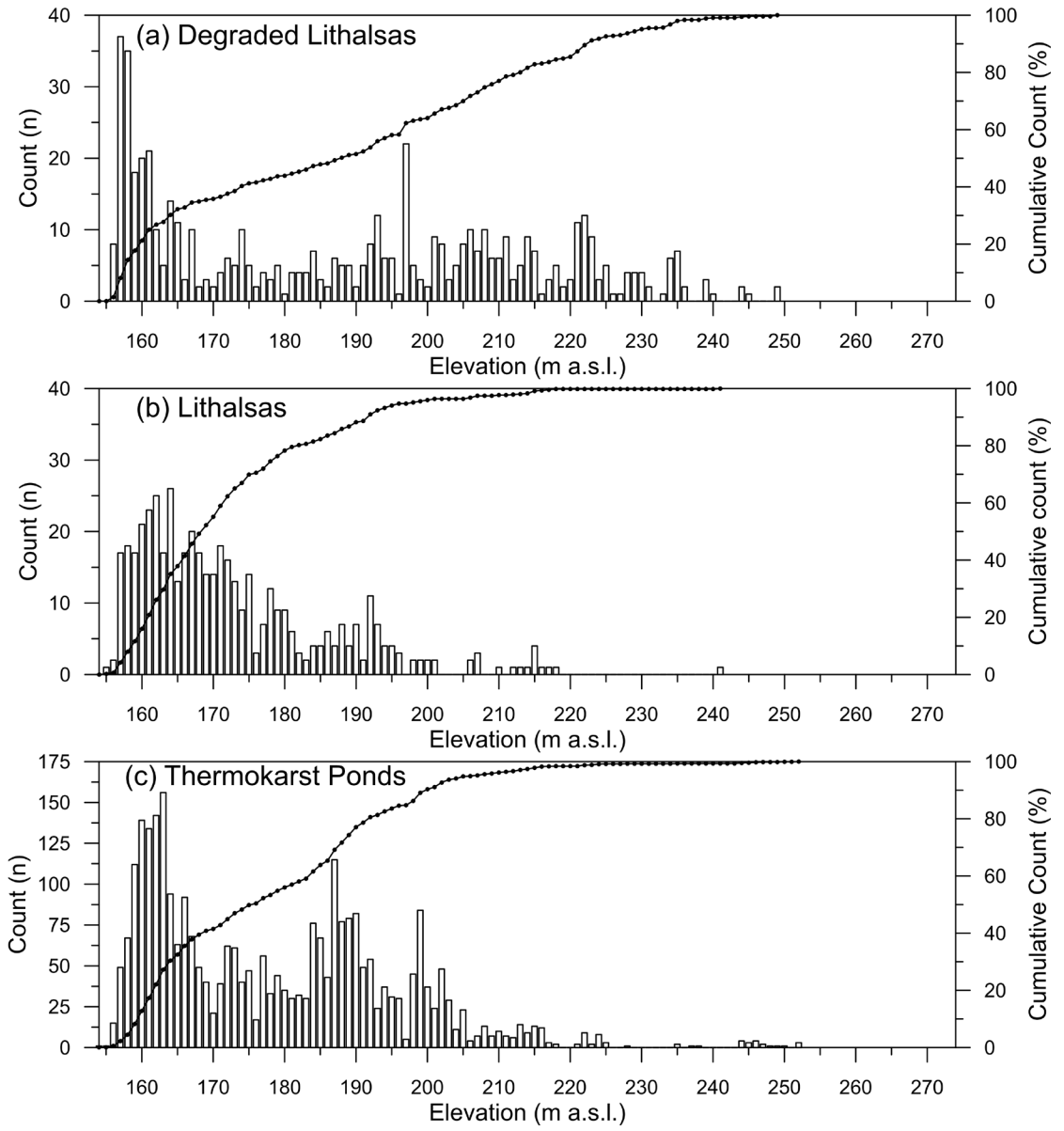

Figure 7. Frequency distributions of (a) degraded lithalsas, (b) lithalsas, and (c) thermokarst ponding with respect to elevation.

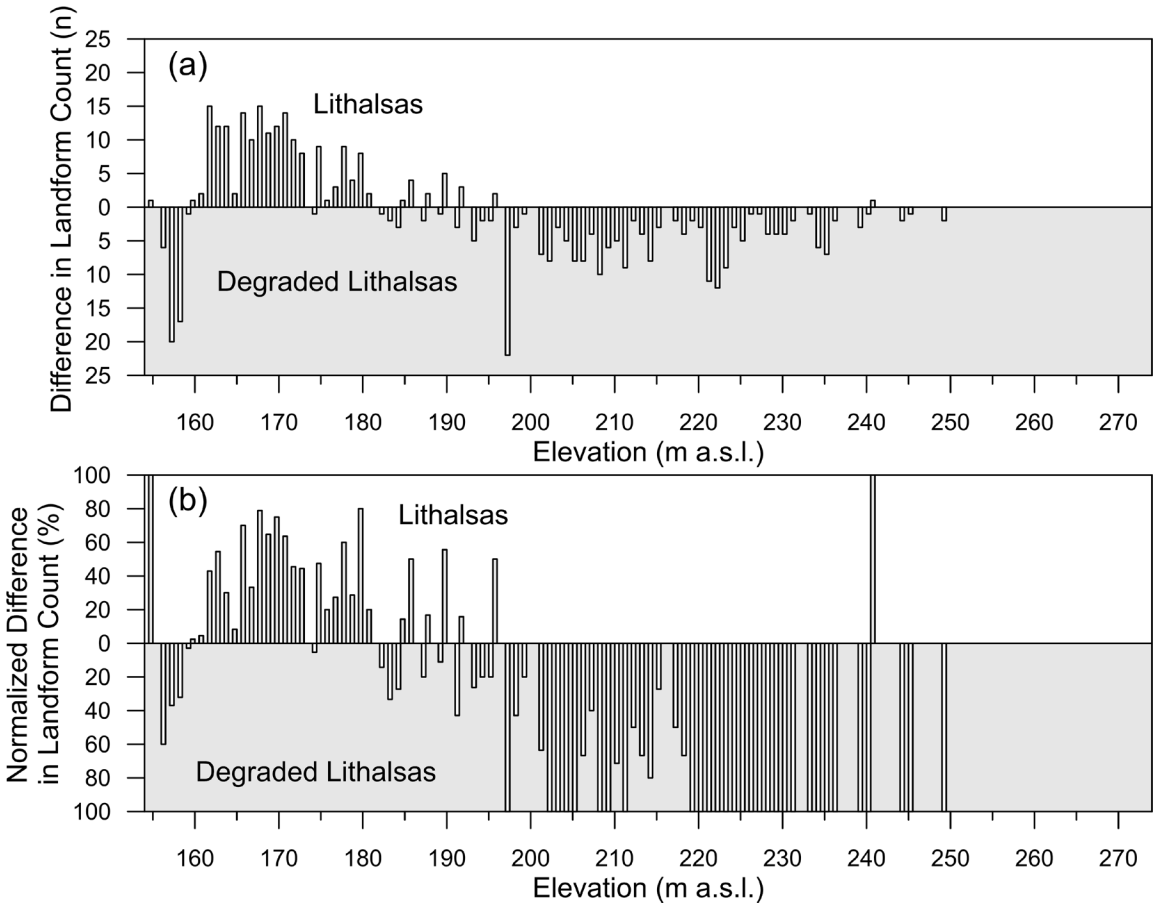

Figure 8. Difference with respect to elevation between lithalsas and degraded lithalsas in terms of (a) count and (b) normalization.

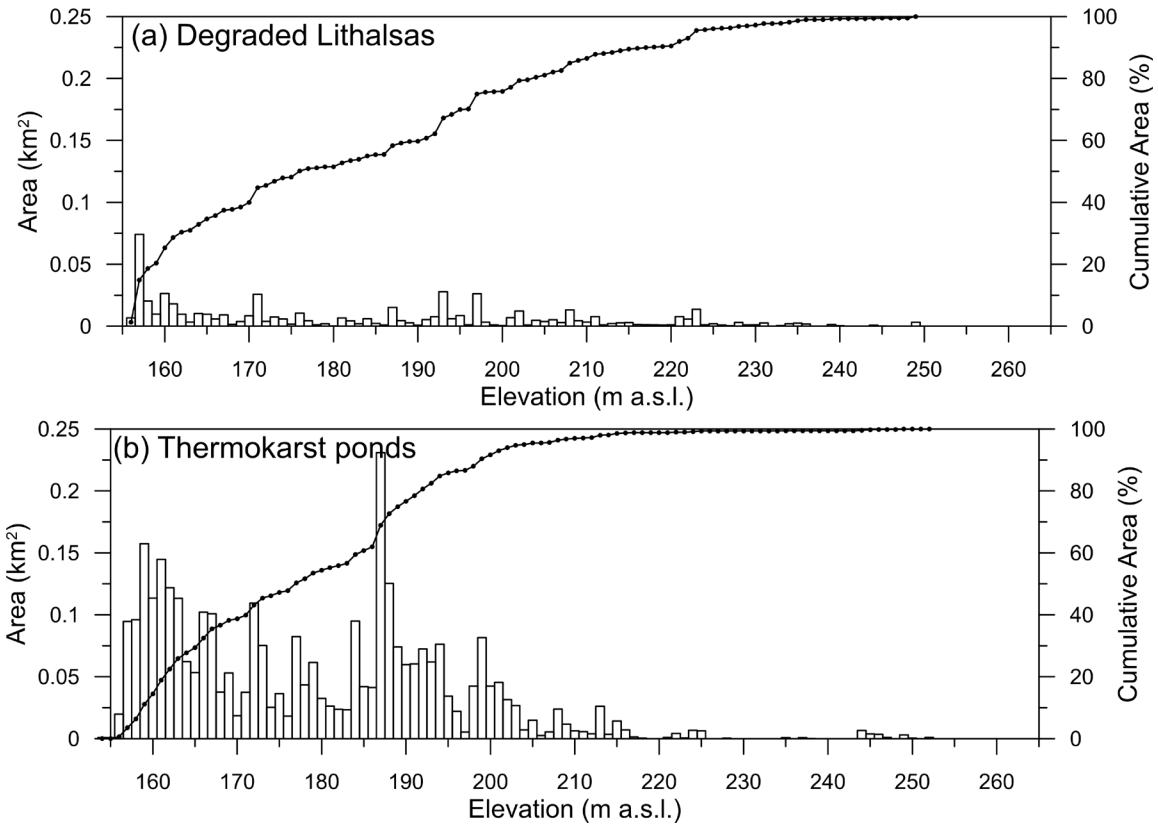

Figure 9. Distributions of area versus elevation for (a) degraded lithalsa ponds (0.54 km^2 total) and (b) thermokarst (1945-2005) ponding (3.33 km^2 total).

Figures 6b and 10 show the relations between surficial geology, degraded and intact lithalsas, and recent thermokarst ponding, and they demonstrate the thaw sensitivity of fine-grained glaciolacustrine deposits. Overall, 72% of degraded lithalsas, 88% of intact lithalsas, and 75% of recent thermokarst ponding occurs in glaciolacustrine deposits. Nearly 20% (n = 800) of all points have water as a surficial geology attribute following the overlay operation in the GIS. This is because there is a high likelihood that many centroids fall on water, which is due to a combination of five factors: (i) lithalsas develop adjacent to water bodies (Gaanderse et al. 2018); (ii) the centroid points extracted from polygons may lie outside of the polygon (many polygons are irregularly shaped); (iii) the water bodies related to degraded lithalsas and the thermokarst ponding would have been mapped as water in the surficial geology map (the surficial geology data are derived from more recent satellite image data than 2005); (iv) water bodies are extensive at all elevations (Figure 11f); and (v) the scale of surficial geology mapping is 1:50000 versus the 1:2500 scale for feature mapping. Visual inspection of numerous points classed as water indicates the closest other surficial geology unit is usually glaciolacustrine sediments.

5.3 **Implications**

As with contemporary thermokarst pond development, most lithalsas (degraded or intact) occur below 200 m a.s.l. in GSL, where glaciolacustrine deposits are commonplace at the expense of bedrock outcropping (Figure 11a, b). The extent of degraded lithalsas throughout the study area, and the near absence of intact lithalsas above 200 m a.s.l. highlights the vulnerability of lithalsas to thaw. It is not clear if the majority of lithalsas at higher elevations have degraded because they have had more time to do so, or the contained less ice to degrade, or both. The high concentrations of degraded and intact lithalsas in GSL lends further support to the hypothesis of Gaanderse et al. (2018) that irrespective of past climate and disturbance effects on lithalsa growth and decay, they are preferentially associated with alluvium, which increased substantially in distribution in the GSL during the late Holocene. Alluvium occurs as at a scale not mapped by Stevens et al (2012b), however, alluvium is deposited on top of the glaciolacustrine sediments near water courses (Gaanderse et al. 2018).

With respect to future infrastructure development in this region, the distributions of lithalsas (degraded and intact) thermokarst ponding suggest that glaciolacustrine deposits should be avoided as this terrain is likely the most sensitive to climate warming and disturbance.

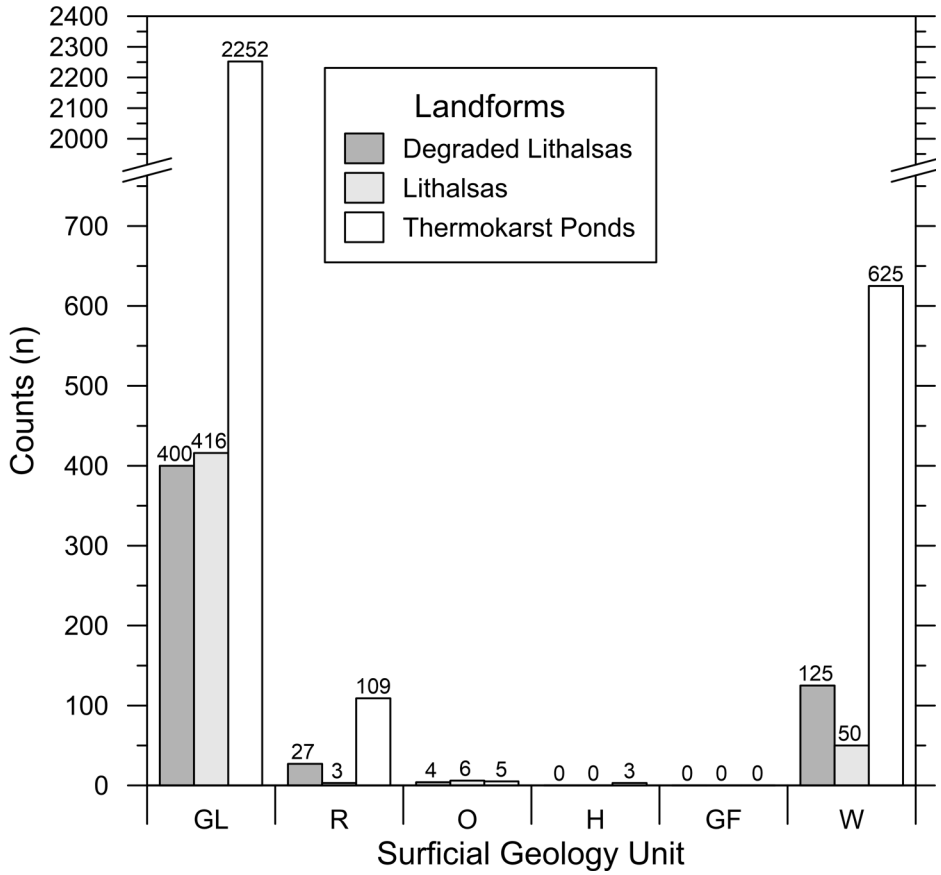

Figure 10. Frequency distributions of degraded lithalsas, lithalsas, and thermokarst ponding (1945-2005) with respect to surficial geology (GL = Glaciolacustrine; R = Rock; O = Organic; H = Anthropogenic; GF = Glaciofluvial; W = Water).

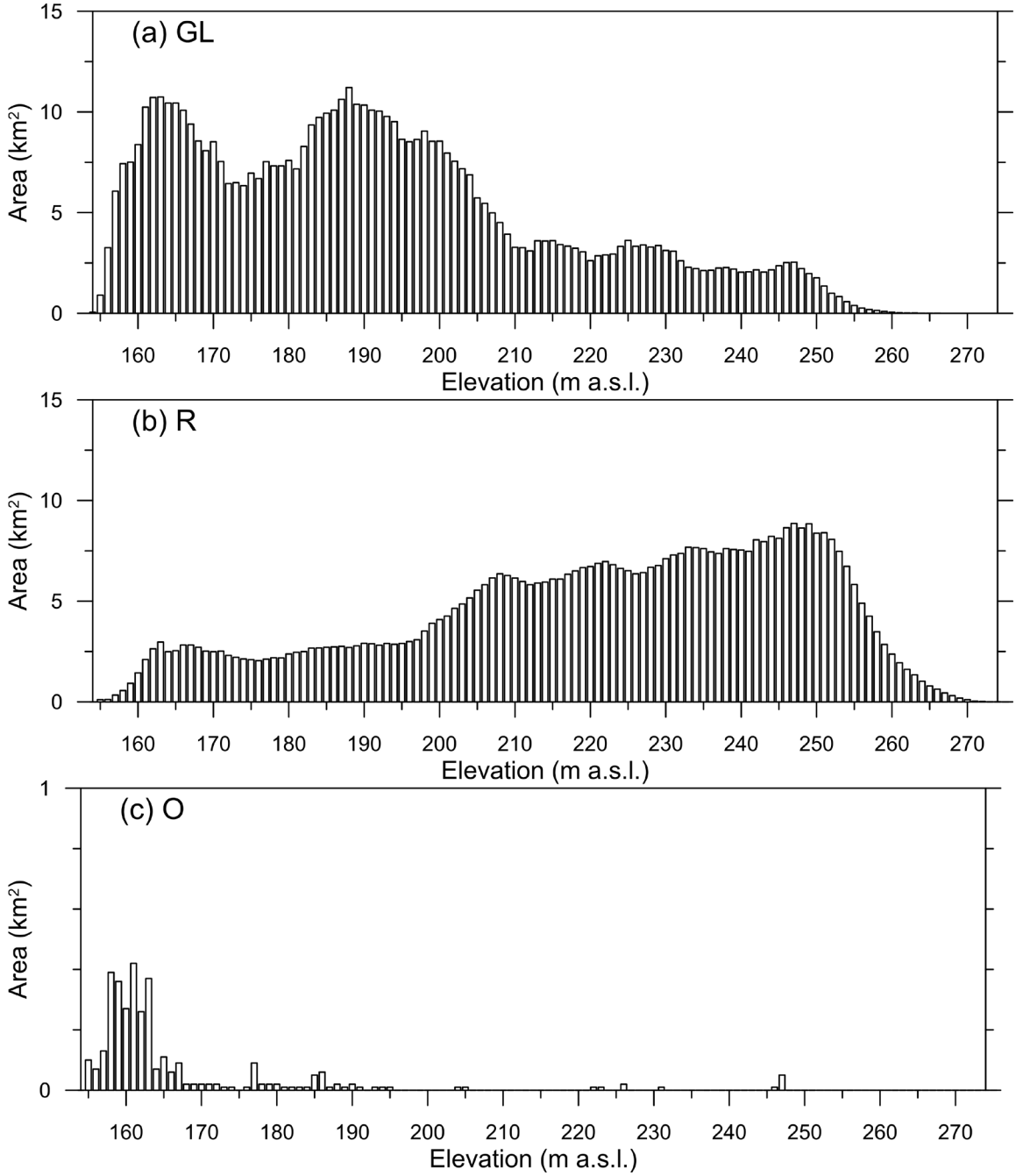

Figure 11. Distributions of area versus elevation for: (a) Glaciolacustrine (G); (b) Bedrock (R); (c) Organic (O); (d) Anthropogenic (H); (e) Glaciofluvial (GF); and (f) Water (W).

Note the change in scale on (a) and (b) versus the remaining panels. Figure continues on the next page.

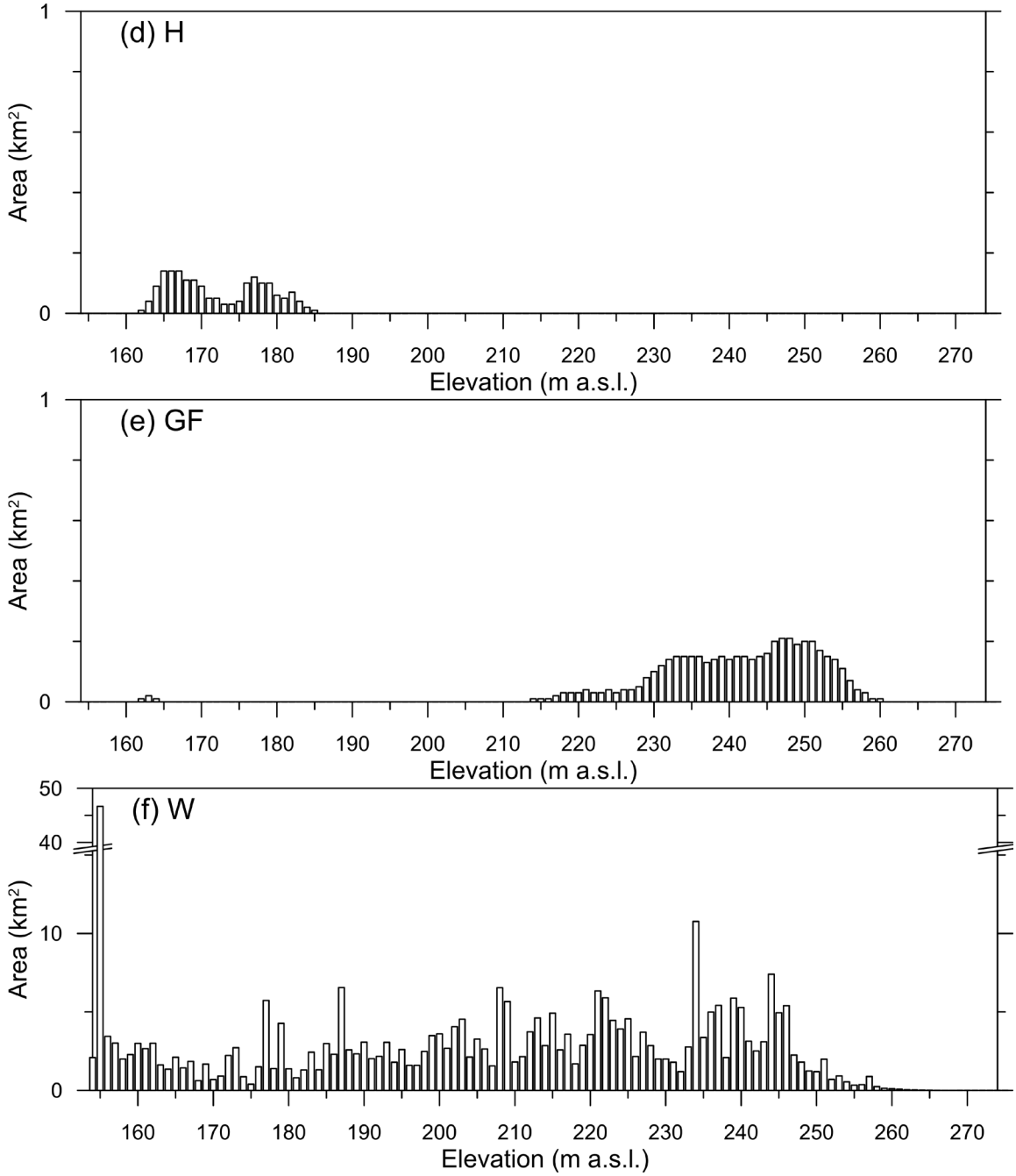

Figure 11. Continued.

6 SUMMARY AND CONCLUSIONS

This Open File provides an inventory of degraded lithalsas, the first of its kind to the authors' knowledge, which was derived from very high-resolution optical satellite images. Further to this, we extend an earlier inventory of lithalsas (Stevens et al. 2012a) so that lithalsa mapping is complete for the present study area. Finally, we re-present thermokarst pond data from Morse et al. (2017) to provide context and to present changes to the dataset owing to the use of an improved digital elevation model (see Appendix A). We find that degraded lithalsas, indicated by a rampart that encloses a thaw pond (which often has standing dead vegetation) are widespread throughout the study area, including above 200 m a.s.l., where intact lithalsas are almost completely absent. Lithalsa (degraded and intact) distribution is related to glaciolacustrine deposits that be come more widespread below about 205 m a.s.l., mainly at the expense of bedrock outcropping. Lithalsas were once much more numerous than at present, but roughly half of them have degraded completely. Many of the remaining lithalsa are visibly degrading. These data, together with contemporary thermokarst ponding (1945-2005) data, demonstrate that glaciofluvial deposits are thaw sensitive and will likely be susceptible to thermal disturbances as a result of climate warming or construction activities.

ACKNOWLEDGMENTS

This research was completed while ACAR was with the Geological Survey of Canada (GSC) via NRCan's Postdoctoral Research Program, and it is a contribution to the GSC's Climate Change Geoscience Program. The authors would like to thank Dr. Stephen Wolfe for helpful discussions and Caroline Duchesne for a thoughtful review.

DATA

The data for degraded lithalsas, intact lithalsas, and thermokarst ponding (1945-2005) are included with this multi-part Open File as GIS-ready ESRI shapefiles. Metadata for these data are presented in Appendix B.

REFERENCES

Brown RJE. 1973. Influence of climatic and terrain factors on ground temperatures at three locations in the permafrost region of Canada. In *Proceedings of the Second International Conference on Permafrost, North American Contribution*, 13–28 July 1973, Yakutsk, USSR. National Academy of Sciences: Washington, DC, USA; 27–34.

Calmels F, Allard M, Delisle G. 2008. Development and decay of a lithalsa in Northern Québec: a geomorphological history. *Geomorphology* **97**: 287–299.

Dionne JC. 1978. Forms et phénomènes périglaciaires en Jamésie, Québec subarctique. *Géographie physique et Quaternaire* **32**: 187-247.

Ecosystem Classification Group. 2008. *Ecological Regions for the Northwest Territories – Taiga Shield*. Government of the Northwest Territories: Yellowknife, NT, Canada; 149 pp.

Environment Canada. 2020. Climate Data Online. http://climate.weather.gc.ca/ [27 November 2020].

Environment and Natural Resources (ENR). 2015. 14.3 Annual area burned and number of fires. In, *NWT State of the Environment Report*, Environment and Natural Resources, Government of Northwest Territories: Yellowknife, NT, Canada. https://www.enr.gov.nt.ca/en/state-environment/143-annual-area-burned-and-number-fires [Last updated: 29 May 2015].

Gaanderse AJR, Wolfe SA, Burn CR. 2018. Composition and origin of a lithalsa related to lake-level recession and Holocene terrestrial emergence, Northwest Territories, Canada. *Earth Surface Processes and Landforms* **43**: 1032-1043. doi: 10.1002/esp.4302

Harris SA. 1993. Palsa-like mounds developed in a mineral substrate, Fox Lake, Yukon Territory. In *Proceedings*, *Permafrost Sixth International Conference*, 5-9 July 1993, Beijing, China. South China University of Technology Press, Wushan Guangzhan, China.

Heginbottom JA, Dubreuil MA, Harker PA. 1995. Canada-Permafrost. In *National Atlas of Canada*, Fifth Edition. National Atlas Information Service, Natural Resources Canada: Ottawa, ON, Canada; Plate 2.1. MCR 4177.

Huang C, MacDonald GM, Cwynar LC. 2004. Holocene landscape development and climate change in the Low Arctic, Northwest Territories, Canada. *Palaeogeography Palaeoclimatology Palaeoecology* **205**: 221–234. DOI:10.1016/j.palaeo.2003.12.009

Japan Aerospace Exploration Agency (JAXA). 2020. ALOS Global Digital Surface Model "ALOS World 3D - 30m (AW3D30)", Version 3.1. Earth Observation Research Center, Tsukuba, Japan. https://www.eorc.jaxa.jp/ALOS/en/aw3d30/index.htm [accessed January 2021].

MacDonald GM, Edwards TWD, Moser KA, Pienitz R, Smol JP. 1993. Rapid response of treeline vegetation and lakes to past climate warming. *Nature* **361**: 243–246. doi:10.1038/361243a0

Morse PD, Wolfe SA, Kokelj SV, Gaanderse AJR. 2015. The occurrence and thermal disequilibrium state of permafrost in forest ecotopes of the Great Slave Region, Northwest Territories, Canada. *Permafrost and Periglacial Processes* **27**: 145-162. doi:10.1002/ppp.1858

Morse PD, McWade TL, Wolfe SA, 2017. Thermokarst ponding, North Slave region, Northwest Territories. *Geological Survey of Canada, Open File 8205*. Geological Survey of Canada: Ottawa, ON, Canada; 30 pp. doi:10.4095/300531

Morse PD, Wolfe SA, Rudy ACA. 2019. Lithalsa Degradation and Thermokarst Distribution, Subarctic Canadian Shield. In, Cold Regions Engineering 2019: Proceedings of the 18th International Conference on Cold Regions Engineering and the 8th Canadian Permafrost Conference, August 18-22, 2019, Quebec City, Canada, Bilodeau, J-P, Nadeau DF, Fortier D, and Conciatori D (eds.). American Society of Civil Engineers: Reston, Virginia; p. 308-316.

Moser KA, MacDonald GM. 1990. Holocene vegetation change at treeline Northwest Territories, Canada. *Quaternary Research* **34**: 227–239. doi:10.1016/0033-5894(90)90033-h

Natural Resources Canada (NRCan). 2019. High Resolution Digital Elevation Model (HRDEM) - CanElevation Series. Government of Canada, https://open.canada.ca/data/en/dataset/957782bf-847c-4644-a757-e383c0057995 [accessed January 2021].

Paul JR, Kokelj SV, Baltzer JL. 2021. Spatial and stratigraphic variation of near-surface ground ice in discontinuous permafrost of the taiga shield. *Permafrost and Periglacial Processes* **32**:3–18. doi:10.1002/ppp.2085

Pissart A. 2002. Palsas, lithalsas and remnants of these periglacial mounds. A progress report. *Progress in Physical Geography* 26:605-621. doi:10.1191/0309133302pp354ra

Pissart A, Calmels F, Wastiaux C. 2011. The potential lateral growth of lithalsas. *Quaternary Research* **75**:371–377

Riseborough, DW, Wolfe SA, and Duchesne C. 2013. Permafrost modelling in northern Slave region Northwest Territories, Phase 1: Climate data evaluation and 1-d sensitivity analysis. *Geological Survey of Canada, Open File 7333*. Geological Survey of Canada: Ottawa, ON, Canada; 50 pp. doi:10.4095/292366

Stevens CW, Wolfe SA, Gaanderse AJR. 2012a. Lithalsa distribution, morphology and landscape associations in the Great Slave Lowlands, Northwest Territories. *Geological Survey of Canada, Open File 7255*. Geological Survey of Canada: Ottawa, ON, Canada; 41 pp. doi:10.4095/292115

Stevens CW, Kerr DE, Wolfe SA, Eagles S. 2012b. Predictive surficial materials and geology derived from LANDSAT 7, Yellowknife, NTS 85 J, Northwest Territories. *Geological Survey of Canada, Open File 7108*. Geological Survey of Canada: Ottawa, ON, Canada; 31 pp. doi:10.4095/291731

Wolfe SA, Morse PD. 2017. Lithalsa formation and Holocene lake-level recession, Great Slave Lowland, Northwest Territories. In: Papers Presented to Commemorate the Legacy to Permafrost Science of Professor J. Ross Mackay (1915–2014), Burn, C. R. (ed). *Permafrost and Periglacial Processes* **28**: 573-579. doi:10.1002/ppp.1901

Wolfe SA, Morse PD, Kokelj SV, Gaanderse AJ. 2017. Great Slave Lowland: The Legacy of Glacial Lake McConnell. In, *Landscapes and Landforms of Western Canada*, Slaymaker O. (ed.). Springer International Publishing, Switzerland; p. 87-96.

Wolfe SA, Morse PD, Hoeve TE, Sladen WE, Kokelj SV, Arenson LU. 2015. Disequilibrium permafrost conditions on NWT Highway 3. Paper 115 in, *Proceedings, 68rd Canadian Geotechnical Conference and 7th Canadian Permafrost Conference*, Quebec City, Quebec. Canadian Geotechnical Society, Richmond, BC; 8 pp.

Wolfe SA, Stevens CW, Gaanderse AJ, Oldenborger GA. 2014. Lithalsa distribution, morphology and landscape associations in the Great Slave Lowland, Northwest Territories, Canada. *Geomorphology* **204**: 302-313. doi:10.1016/j.geomorph.2013.08.014

Zhang Y, Olthof I, Fraser R., Wolfe SA. 2014. A new approach to mapping permafrost and change incorporating uncertainties in ground conditions and climate projections. *The Cryosphere* **8**: 2177-2194. doi:10.5194/tc-8-2177-2014

Zhang Y, Wolfe SA, Morse PD, Olthof I, Fraser RH. 2015. Spatiotemporal impacts of wildfire and climate warming on permafrost across a subarctic region, Canada. *Journal of Geophysical Research: Earth Surface* **120**: 2338-2356. doi:10.1002/2015JF003679

APPENDIX A – Hybrid Digital Elevation Model for the Study Area

Due to satellite orbital patterns and mission goals, there are comparatively few continental-to-global scale digital elevation models (DEMs) with extents that cover areas north of 60° latitude. Earlier investigations of relations between lithalsas and thermokarst (Morse et al. 2017, Wolfe and Morse 2017, Morse et al. 2019) used the high-resolution Canada Digital Elevation Model (CDEM) to investigate relations between geomorphology and elevation as the CDEM was the model supported by Natural Resources Canada at the time. The horizontal resolution of CDEM is 30 m in the study area, with 1 m vertical resolution. CDEM is not without deficiencies as it was compiled from mainly hypsographic and hydrographic elements of the National Topographic Data Base (NTDB) at the scale of 1:50 000 (NRCan 2013). The NTDB database compiles topographic data from map sheets that were produced independently, and with variable elevation units (feet versus metres), and contour interval spacing. Consequently, elevation contours do not always edge-match between map sheets, and elevation offsets at map sheet boundaries are common artifacts in the CDEM (Figure A1). Further to this, CDEM exhibits a distinct spatial pattern in the elevation data such that elevation values appear to cluster at elevations corresponding to primary topographic contour intervals (Figure A2a). This pattern is likely a result of generating the elevation model from hypsographic elements. CDEM is now considered to be a legacy product that is no longer supported.

CDEM is being replaced by High Resolution Digital Elevation Model (HRDEM) (NRCan 2019a), and in the north it is derived mainly from modified ArcticDEM data (Porter et al. 2018). It has very high horizonal (2 m) and vertical (<1 m) resolutions, and several anomalies in the ArcticDEM are corrected in the HRDEM such as lake elevations, which are often erroneous, but numerous data gaps in the ArcticDEM carry through to the HRDEM (Figure A3).

Owing to the anomalies presented in CDEM, we sought to fill in the HRDEM gaps with another free, high resolution DEM with coverage of the Canadian Arctic. To aid DEM processing and analysis, all DEMs were reprojected from their native datums to Coordinate Reference system “EPSG:3580 - NAD83 / NWT Lambert”, thus all elevations are with respect to NAD83. The most widely used DEMs that meet our criteria are Advanced Spaceborne Thermal Emission and Reflection Radiometer Global Digital Elevation Model Version 3 (ASTER GDEM V3) (NASA 2019) and Advanced Land Observing Satellite Global Digital Surface Model "ALOS World 3D - 30m” version 3.1 (ALOS AW3D30) (JAXA 2020). Both are based on optical stereoscopy and are produced at 30-m resolution. However, in evaluations of vertical accuracy, ALOS AW3D30 is demonstrated to have a higher vertical accuracy than ASTER GDEM V3, which has high

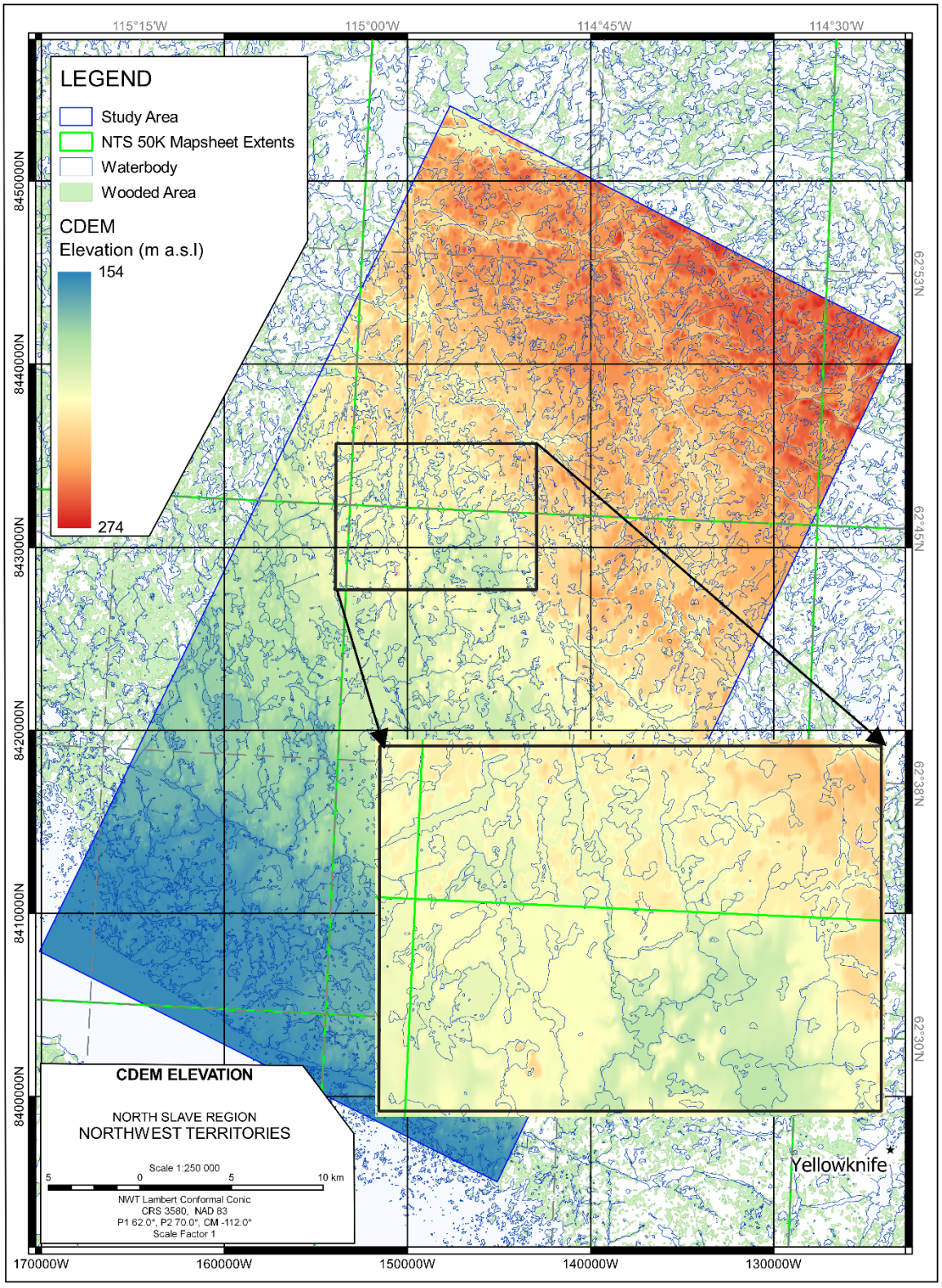

Figure A1. Canada Digital Elevation Model (CDEM) for the study area extent (source: NRCan 2015). The pop out shows artifacts related to map boundaries of topographic data used to generate the elevation model.

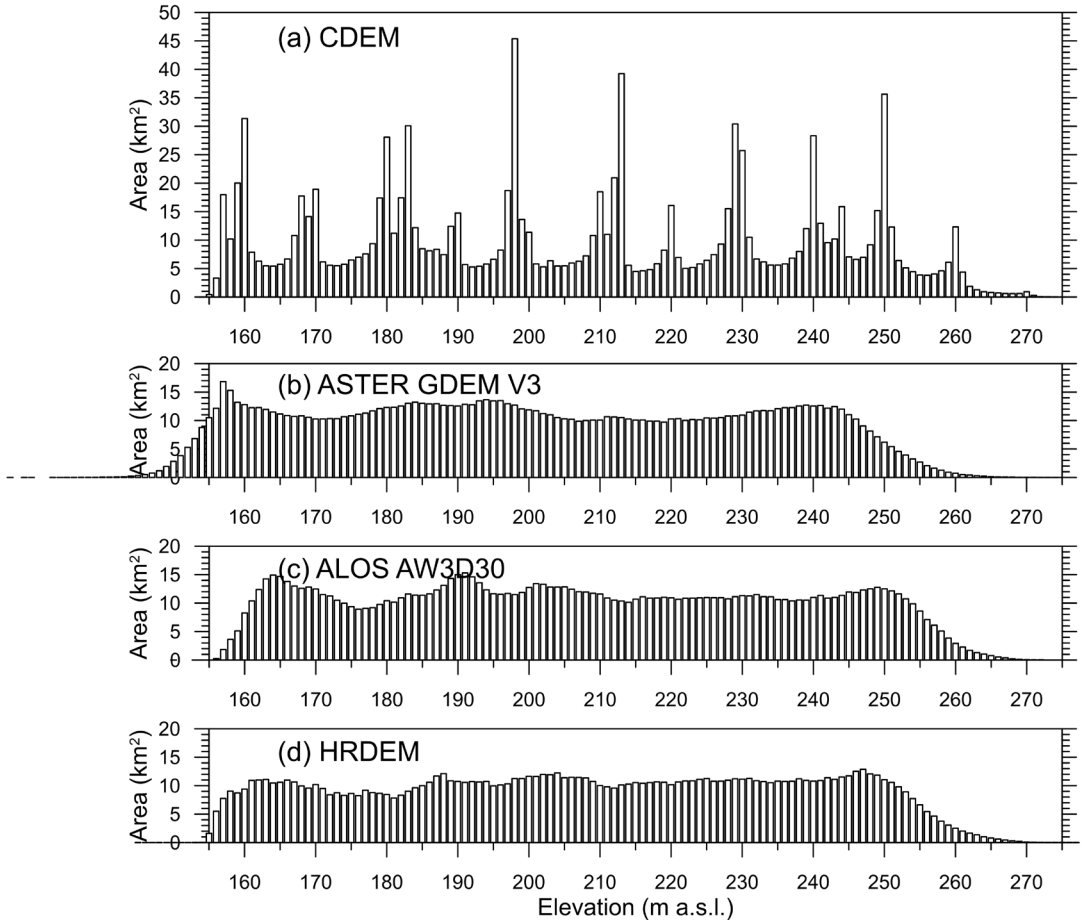

Figure A2. Digital elevation model area versus elevation for land) within the study area (excludes waterbody areas) according to: (a) Canada Digital Elevation Model (CDEM) (NRCan 2015); (b) Advanced Spaceborne Thermal Emission and Reflection Radiometer Global Digital Elevation Model Version 3 (ASTER GDEM V3) (NASA 2019); (b) Advanced Land Observing Satellite Global Digital Surface Model "ALOS World 3D - 30m" (ALOS AW3D30) (JAXA 2020); (c) and High Resolution Digital Elevation Model (HRDEM) (NRCan 2019b). Elevations are with respect to NAD83.

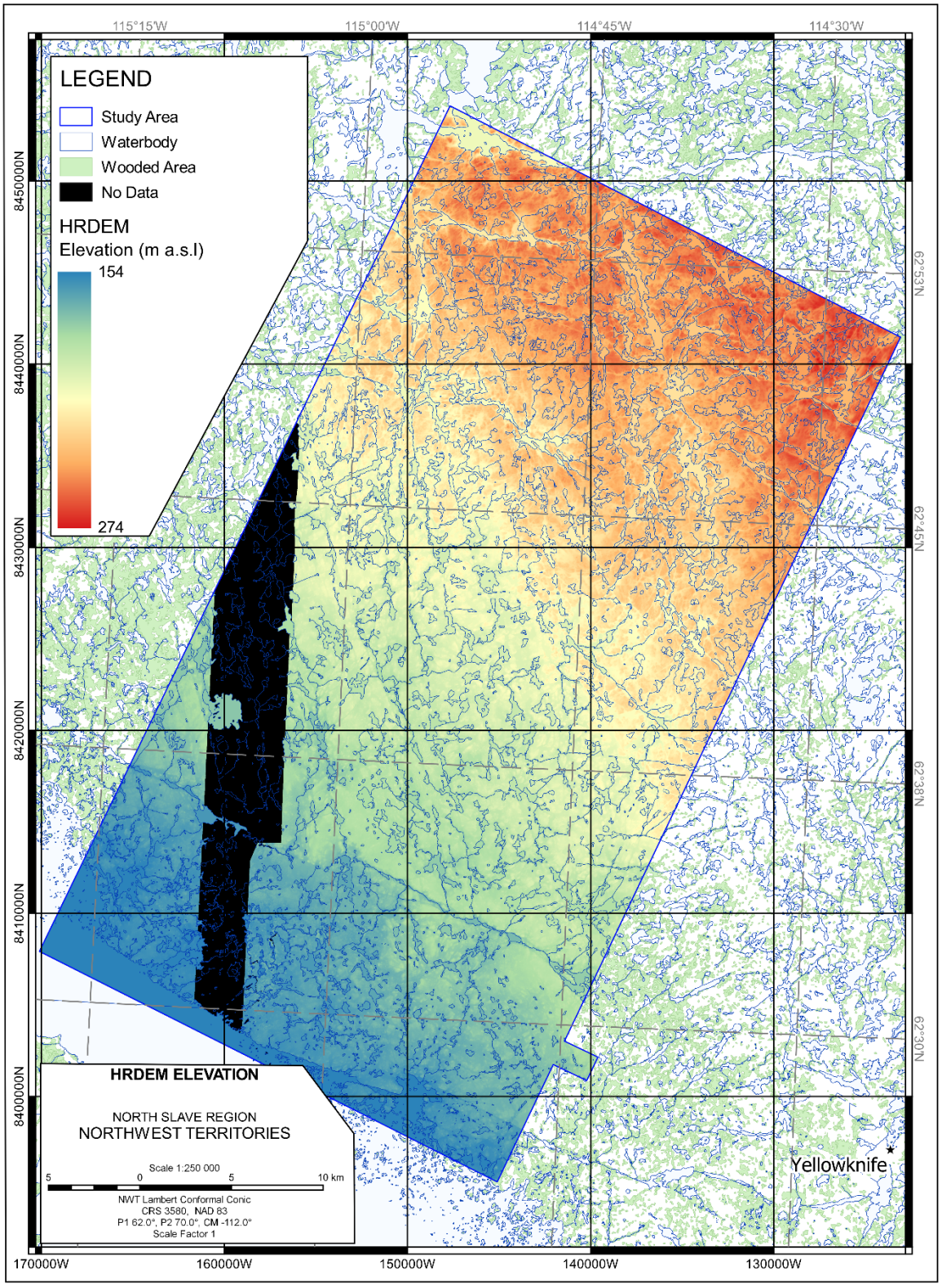

Figure A3. High Resolution Digital Elevation Model (HRDEM) for the study area extent (source: NRCan2019b).

errors and hummock-like patterns distributed in an apparently random manner (e.g., Florinsky et al. 2018). Both DEMs can have errors over water bodies owing to their derivation from optical satellite data.

For the extent of land (does not include waterbodies) in the study area, ASTER GDEM V3 has a noticeable negative shift in elevations with respect to HRDEM and CDEM (Figure A2b), and hummock-like elevation patterns are present (Figure A4). In contrast, ALOS AW3D30 presents an elevation distribution that is comparatively similar to HRDEM for land areas (Figures A2c and A2d), and ALOS AW3D30 only exhibits anomalies over a subset of the waterbodies (Figure A5). Consequently, we filled in the HRDEM data gaps with ALOS AW3D30, which carried with it any anomalies associated with water bodies (Figure A6). Given the problems associated with CDEM, and the lack of other elevation data sufficient to fill in the lake elevations, these anomalies remain. The final composite DEM is 2 m resolution (ALOS AW3D30 pixels were resampled from 30 m to 2 m) and elevations are reported to the nearest metre. Upon visual inspection, the vertical offset between adjacent pixels derived from the two separate DEMs is up to 6 m, but is typically less than 3 m.

The composite DEM was then used to interrogate the geomorphic feature data sets. There are a handful of feature data points that fall on some of the remaining anomalous lake elevation data, but the errors incurred by these points are deemed to be minimal given the scope and aims of the present research and the number of thermokarst pond, lithalsa, and degraded lithalsa features mapped. When the thermokarst pond, lithalsa, and degraded lithalsa datasets are compared with respect to DEM, it is clear that the new composite DEM is an improvement as gross errors associated with the CDEM (Figures A7a, A8a, A9a) are no longer present (Figures A7b, A8b, A9b).

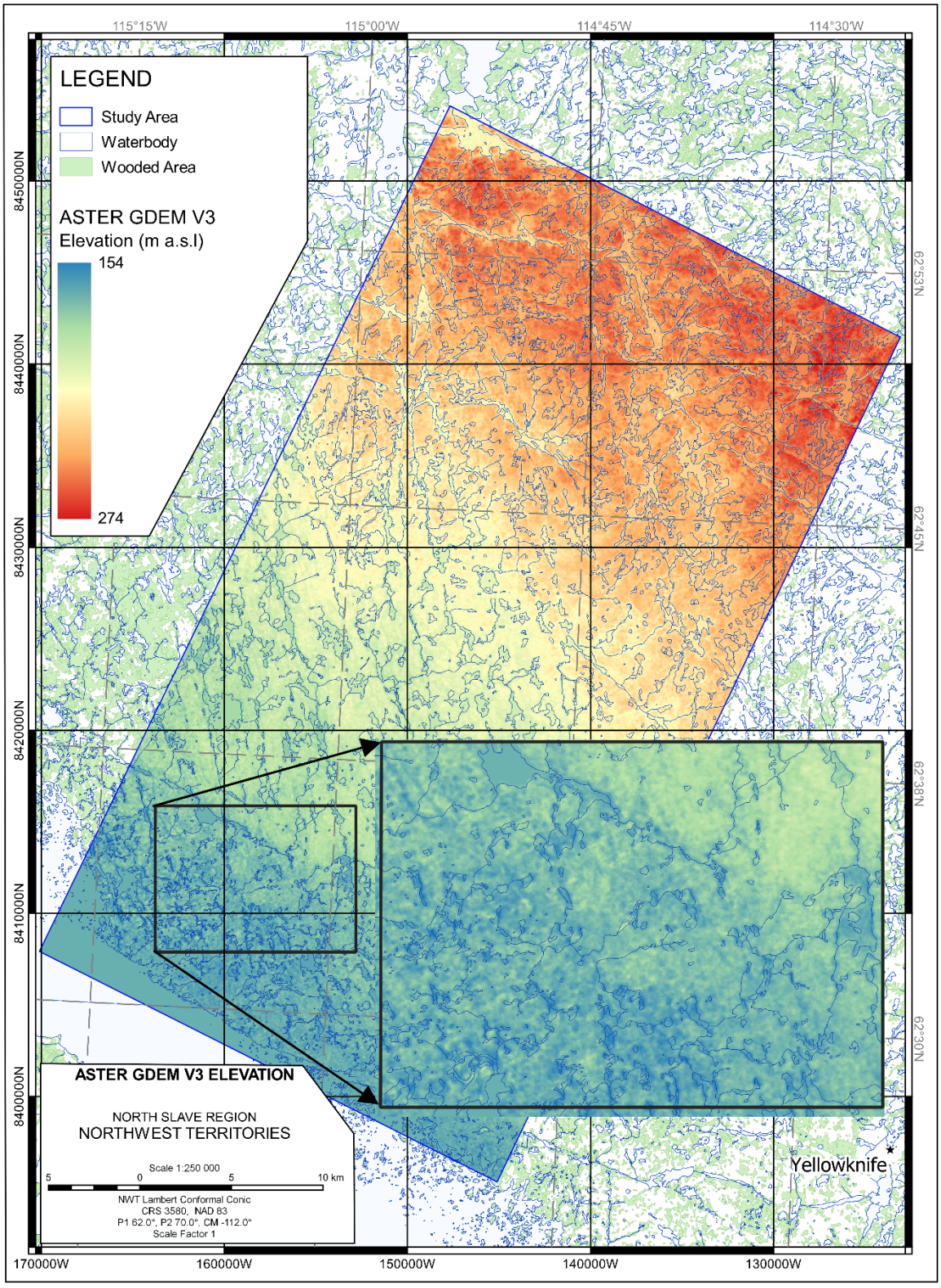

Figure A4. Advanced Spaceborne Thermal Emission and Reflection Radiometer Global Digital Elevation Model Version 3 (ASTER GDEM V3) for the study area extent (source: NASA 2019). The pop out shows "hummock-like" artifacts.

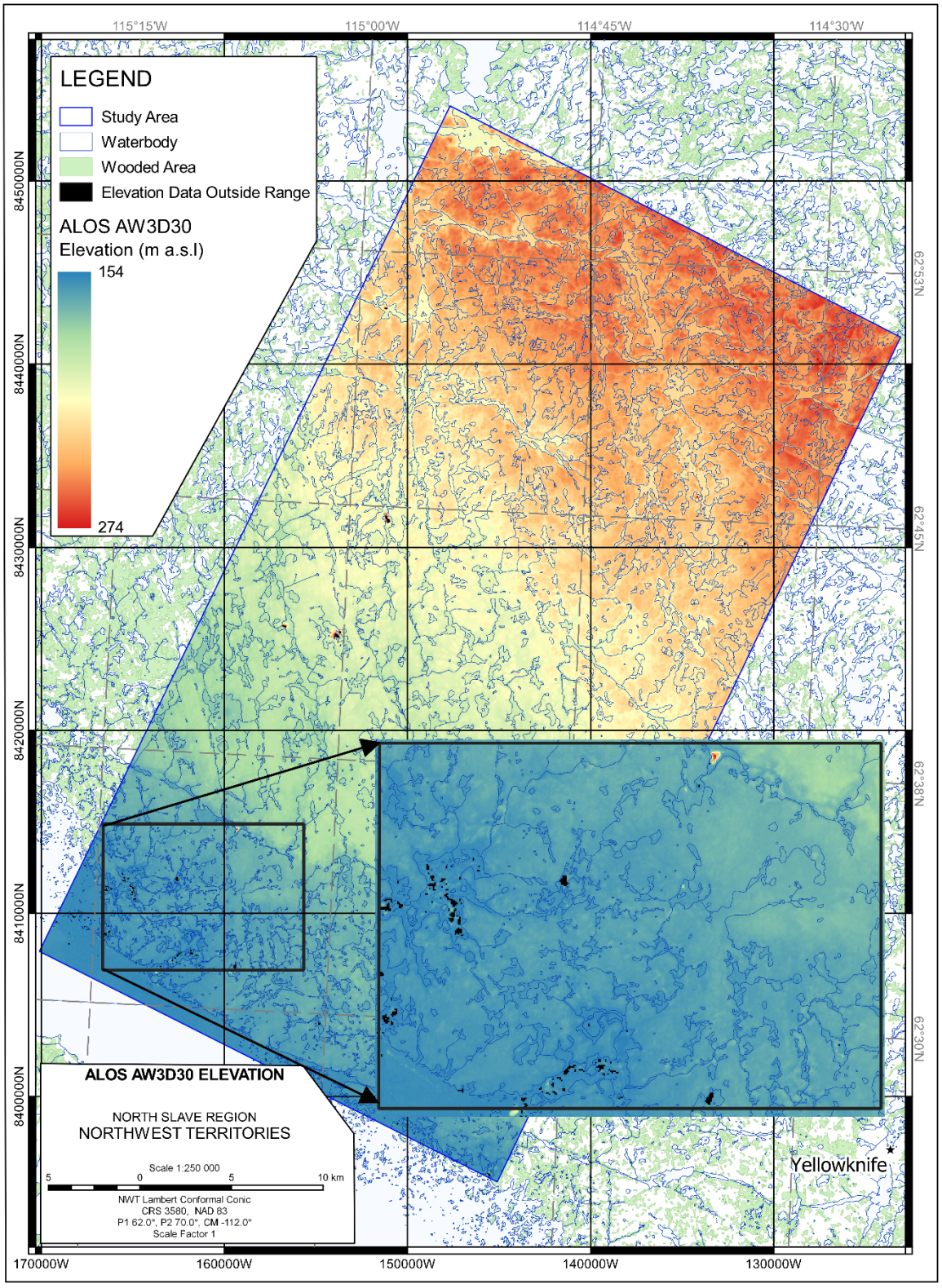

Figure A5. Advanced Land Observing Satellite Global Digital Surface Model "ALOS World 3D - 30m" (ALOS AW3D30) (source: JAXA 2020) for the study area extent. The pop out shows elevation anomalies associated with waterbodies.

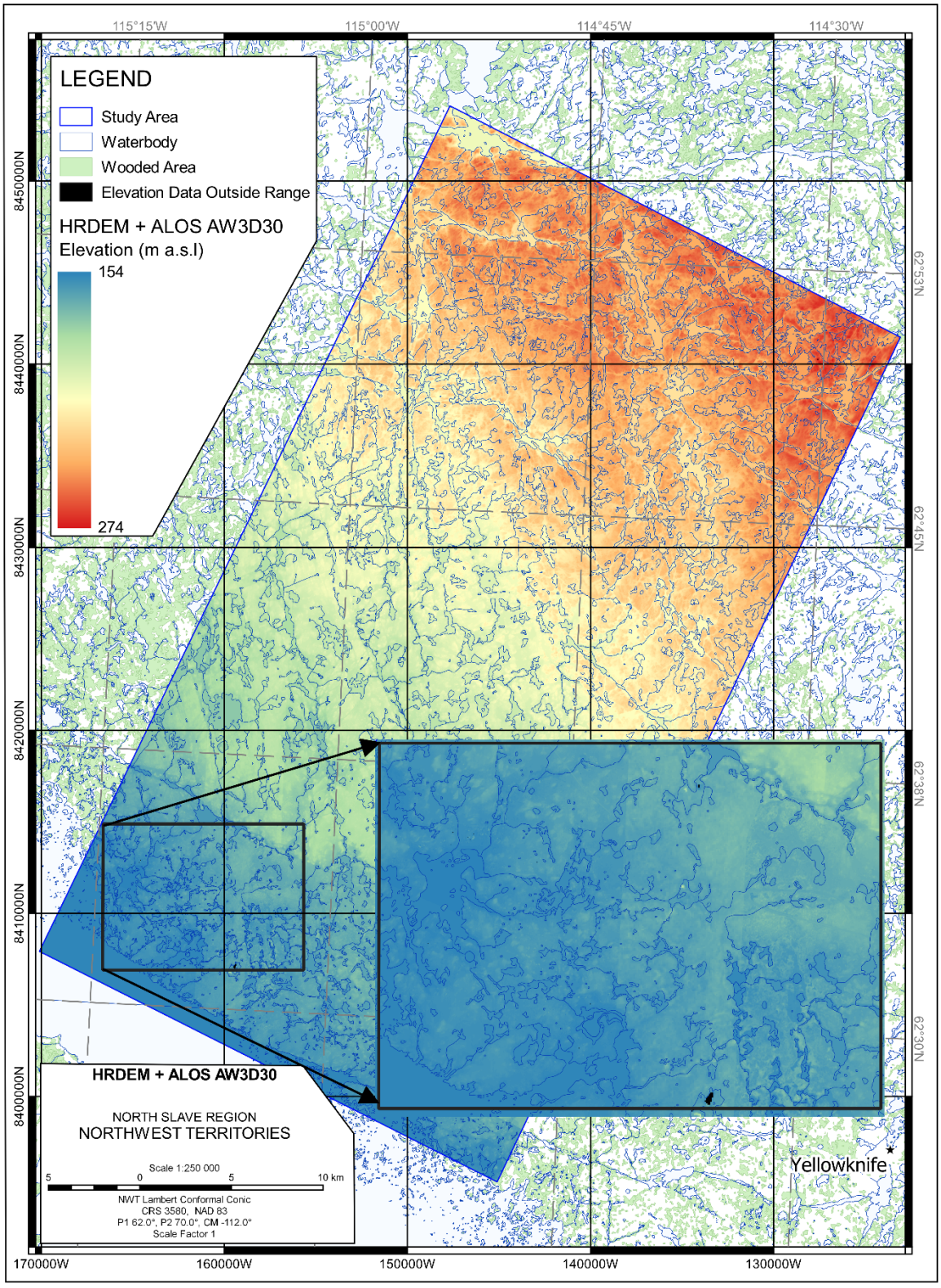

Figure A6. Composite DEM (HRDEM + ALOS AW3D30) for the study area extent.

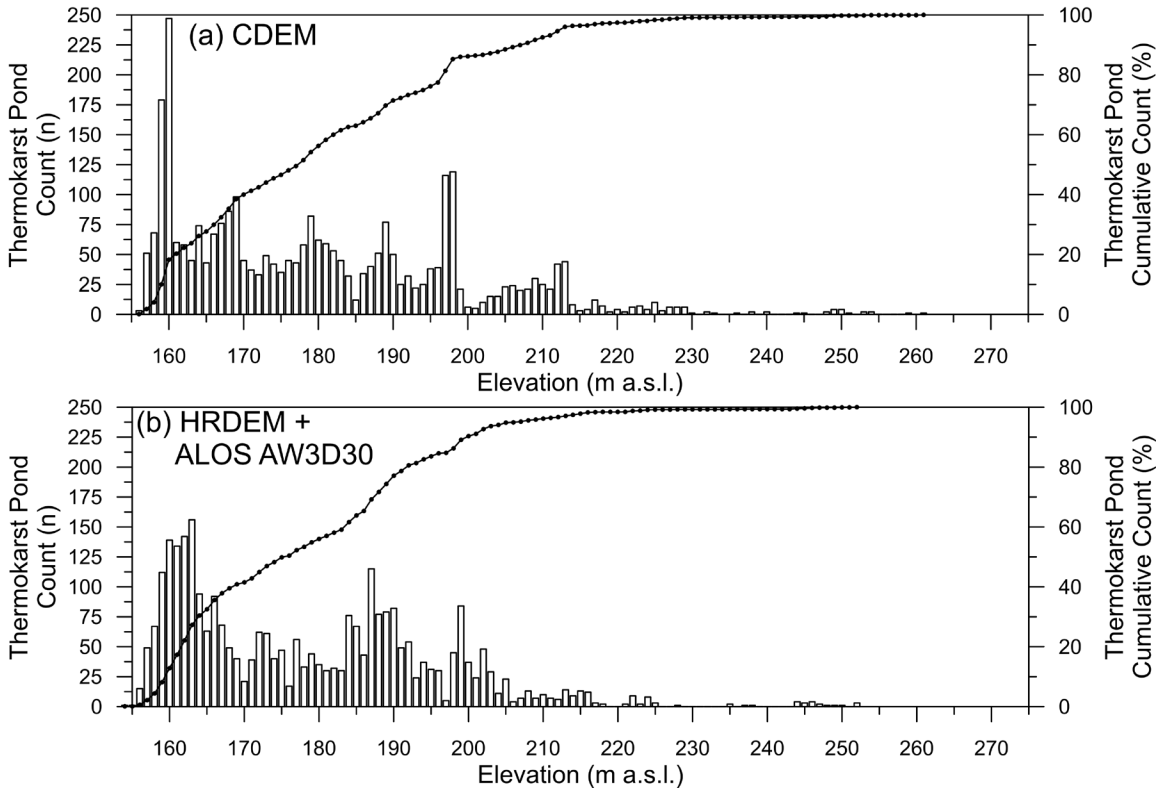

Figure A7. Counts of thermokarst ponds versus elevation according to (a) CDEM and (b) the composite DEM.

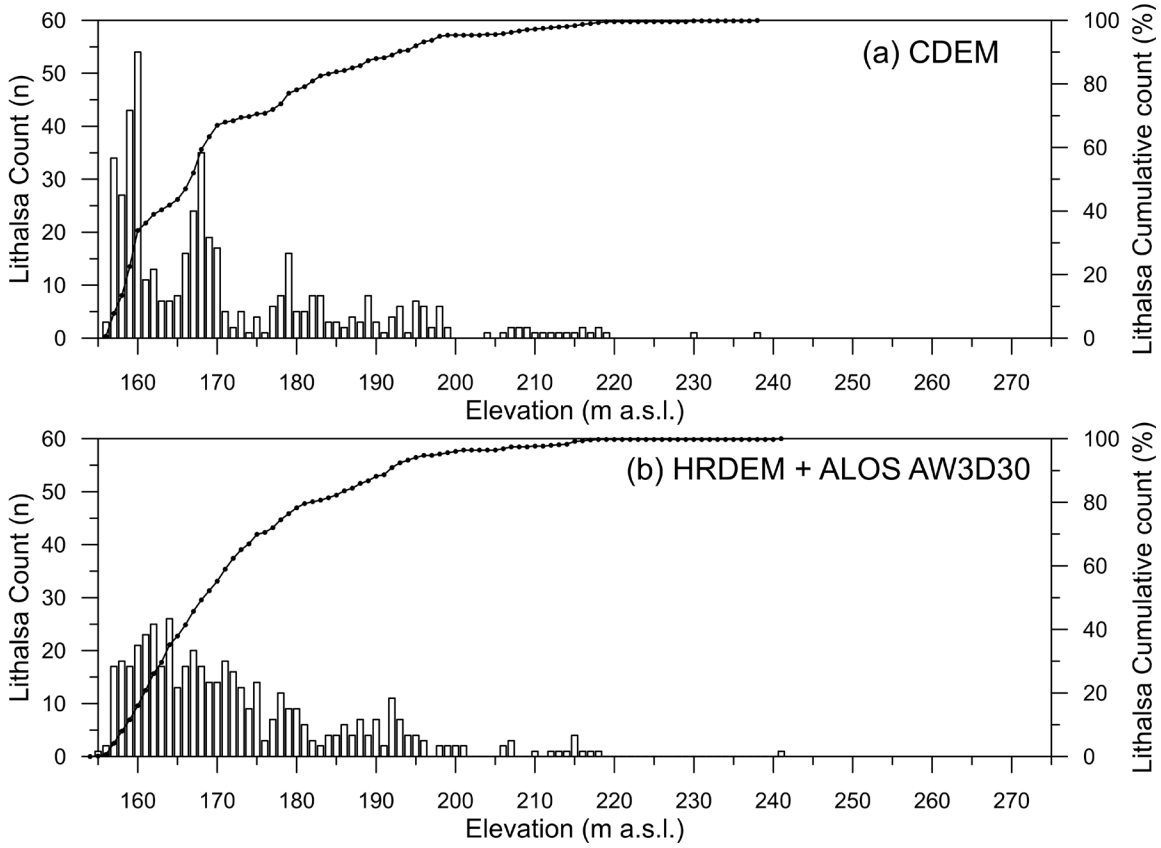

Figure A8. Counts of lithalsas versus elevation according to (a) CDEM and (b) the composite DEM.

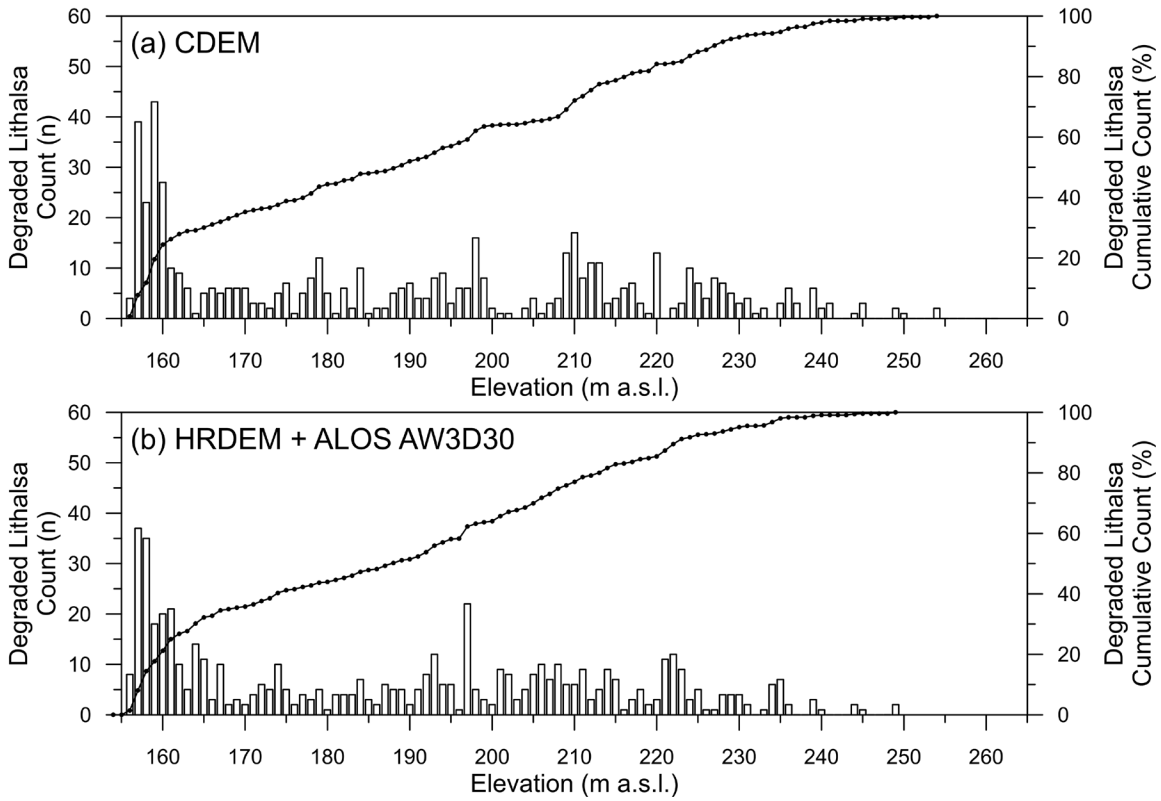

Figure A9. Counts of degraded lithalsas versus elevation according to (a) CDEM and (b) the composite DEM.

References:

Florinsky IV, Skrypitsyna TN, Luschikova OS. 2018. Comparative accuracy of the AW3D30 DSM, ASTER GDEM, and SRTM1 DEM: A case study on the Zaoksky testing ground, Central European Russia. *Remote Sensing Letters* **9**:706-714. doi: 10.1080/2150704X.2018.1468098

Japan Aerospace Exploration Agency (JAXA). 2020. ALOS Global Digital Surface Model "ALOS World 3D - 30m (AW3D30)", Version 3.1. Earth Observation Research Center, Tsukuba, Japan. https://www.eorc.jaxa.jp/ALOS/en/aw3d30/index.htm [accessed January 2021].

Morse PD, McWade TL, Wolfe SA. 2017. Thermokarst ponding, North Slave region, Northwest Territories. *Geological Survey of Canada, Open File 8205*. Geological Survey of Canada: Ottawa, ON, Canada; 30 pp. doi:10.4095/300531

Morse PD, Wolfe SA, Rudy ACA. 2019. Lithalsa Degradation and Thermokarst Distribution, Subarctic Canadian Shield. In, Cold Regions Engineering 2019: Proceedings of the 18th International Conference on Cold Regions Engineering and the 8th Canadian Permafrost Conference, August 18-22, 2019, Quebec City, Canada, Bilodeau, J-P, Nadeau DF, Fortier D, and Conciatori D (eds.). American Society of Civil Engineers: Reston, Virginia; p. 308-316.

Natural Resources Canada (NRCan). 2013. Canadian Digital Elevation Model Product Specifications, Ed. 1.1. Canada Centre for Mapping and Earth Observation, Client Services, 50 Place de la Cité, Suite 212, Sherbrooke, Quebec, Canada; 18 pp.

Natural Resources Canada (NRCan). 2015. Canadian Digital Elevation Model, 1945-2011. Government of Canada, https://open.canada.ca/data/en/dataset/7f245e4d-76c2-4caa-951a-45d1d2051333 [accessed January 2021].

Natural Resources Canada (NRCan). 2019a. High Resolution Digital Elevation Model (HRDEM) – CanElevation Series – Product Specifications, Ed. 1.3. Canada Centre for Mapping and Earth Observation, Client Services, 50 Place de la Cité, Suite 212, Sherbrooke, Quebec, Canada; 20 pp.

Natural Resources Canada (NRCan). 2019b. High Resolution Digital Elevation Model (HRDEM) - CanElevation Series. Government of Canada, https://open.canada.ca/data/en/dataset/957782bf-847c-4644-a757-e383c0057995 [accessed January 2021].

Porter C, Morin P, Howat I, Noh M-J, Bates B, Peterman K, Keesey S, Schlenk M, Gardiner J, Tomko K, Willis M, Kelleher C, Cloutier M, Husby E, Foga S, Nakamura H, Platson M, Wethington M Jr., Williamson C, Bauer G, Enos J, Arnold G, Kramer W, Becker P, Doshi A, D'Souza C, Cummens P, Laurier F, Bojesen M. 2018. ArcticDEM. https://doi.org/10.7910/DVN/OHHUKH, Harvard Dataverse, V1, [accessed December 2020].

United States National Aeronautics and Space Administration (NASA). 2019. Advanced Spaceborne Thermal Emission and Reflection Radiometer (ASTER). Jet Propulsion

Laboratory, California Institute of Technology, Pasadena, CA. https://asterweb.jpl.nasa.gov/ [accessed January 2021].

Wolfe SA, Morse PD. 2017. Lithalsa formation and Holocene lake-level recession, Great Slave Lowland, Northwest Territories. In: Papers Presented to Commemorate the Legacy to Permafrost Science of Professor J. Ross Mackay (1915–2014), Burn, C. R. (ed). *Permafrost and Periglacial Processes* **28**: 573-579. doi:10.1002/ppp.1901

APPENDIX B - METADATA

of8869_points


```
<!DOCTYPE qgis PUBLIC 'http://mrcc.com/qgis.dtd' 'SYSTEM'>

<qgis version="3.10.7-A Coruña">


<identifier>of_8869\Data\degradedlithalsa_lithalsa_thermokarst_points\of8869_points.shp</identifier>

  <parentidentifier>Morse, P.D., Rudy, A.C.A, 2022. Distributions of degraded and intact lithalsas, North Slave region, Northwest Territories; Geological Survey of Canada, Open File 8869, 1 .zip file. doi:10.4095/329643</parentidentifier>

  <language>ENG</language>

  <type>dataset</type>

  <title>Degraded Lithalsa, Lithalsa, and Thermokarst Points</title>

  <abstract> The main objective of this report is to provide an inventory of current (intact or degrading) and old (completely degraded) lithalsas in a representative study area of the southern North Slave region between Behchoko and Yellowknife in the Northwest Territories. A lithalsa is an ice-rich mound of permafrost that causes the soil to settle downward and water to pond if the ice core thaws (thermokarst pond). Lithalsas, widespread in this region, are therefore very sensitive to thawing. This inventory should help to better understand current and future permafrost conditions, and is based directly on the GSC's Open File 7255, which provides an inventory of many lithalsas in the region, as well as on the GSC's Open File 8205, which provides an inventory of thermokarst pond development between 1945 and 2005 in the same study area. Using high-resolution satellite images, we completed the inventory of 475 intact lithalsas in the study area. Then, by combining our field observations of surface
```

geomorphology of degrading lithalsas with recognizable geomorphic patterns in the same satellite imagery, we developed criteria to identify and map them and we developed an inventory of 556 completely degraded lithalsas. The inventories and databases are prepared for assessment of the relations between elevation, surface geology and distribution of lithalsas, and the trajectory of thermokarst development in the region. The inventories included with this report can be used directly in a Geographic Information System (GIS).</abstract>

```
  <keywords vocabulary="gmd:topicCategory">
    <keyword>Environment</keyword>
    <keyword>Geoscientific Information</keyword>
  </keywords>
  <keywords vocabulary="undefined 2">
    <keyword>Lithalsa</keyword>
    <keyword> Thermokarst</keyword>
  </keywords>
  <contact>
    <contactAddress>
      <type>postal</type>
      <address>601 Booth Street</address>
      <city>Ottawa</city>
      <administrativearea>ON</administrativearea>
      <postalcode>K1A 0E8</postalcode>
      <country>Canada</country>
    </contactAddress>
    <name>Peter Morse</name>
```

```
    <organization>Geological Survey of Canada, Natural
Resources Canada</organization>

    <position>Research Scientist</position>

    <voice></voice>

    <fax></fax>

    <email>peter.morse@canada.ca</email>

    <role>owner</role>

  </contact>

  <links>

    <link format="*.zip" mimeType="" type="download" url="
https://doi.org/10.4095/329643" size="" name="GEOSCAN"
description="Open File multi-part report"/>

  </links>

  <fees>None.</fees>

  <rights>© Her Majesty the Queen in Right of Canada, as
represented by the Minister of Natural Resources Canada,
2022.</rights>

  <license>Government of Canada: View the licence agreement
at http://data.gc.ca/eng/open-government-licence-
canada</license>

  <encoding></encoding>

  <crs>

    <spatialrefsys>

      <wkt>PROJCRS["NAD83 / NWT
Lambert",BASEGEOGCRS["NAD83",DATUM["North American Datum
1983",ELLIPSOID["GRS
1980",6378137,298.257222101,LENGTHUNIT["metre",1]]],PRIMEM[
"Greenwich",0,ANGLEUNIT["degree",0.0174532925199433]],ID["E
PSG",4269]],CONVERSION["Northwest Territories
Lambert",METHOD["Lambert Conic Conformal
(2SP)",ID["EPSG",9802]],PARAMETER["Latitude of false
```

```
origin",0,ANGLEUNIT["degree",0.0174532925199433],ID["EPSG",
8821]],PARAMETER["Longitude of false origin",-
112,ANGLEUNIT["degree",0.0174532925199433],ID["EPSG",8822]]
,PARAMETER["Latitude of 1st standard
parallel",62,ANGLEUNIT["degree",0.0174532925199433],ID["EPS
G",8823]],PARAMETER["Latitude of 2nd standard
parallel",70,ANGLEUNIT["degree",0.0174532925199433],ID["EPS
G",8824]],PARAMETER["Easting at false
origin",0,LENGTHUNIT["metre",1],ID["EPSG",8826]],PARAMETER[
"Northing at false
origin",0,LENGTHUNIT["metre",1],ID["EPSG",8827]]],CS[Cartes
ian,2],AXIS["(E)",east,ORDER[1],LENGTHUNIT["metre",1]],AXIS
["(N)",north,ORDER[2],LENGTHUNIT["metre",1]],USAGE[SCOPE["u
nknown"],AREA["Canada - NWT"],BBOX[59.98,-136.46,78.81,-
102]],ID["EPSG",3580]]</wkt>

      <proj4>+proj=lcc +lat_0=0 +lon_0=-112 +lat_1=62
+lat_2=70 +x_0=0 +y_0=0 +ellps=GRS80 +towgs84=0,0,0,0,0,0,0
+units=m +no_defs</proj4>

      <srsid>1538</srsid>

      <srid>3580</srid>

      <authid>EPSG:3580</authid>

      <description>NAD83 / NWT Lambert</description>

      <projectionacronym>lcc</projectionacronym>

      <ellipsoidacronym>EPSG:7019</ellipsoidacronym>

      <geographicflag>false</geographicflag>

    </spatialrefsys>

  </crs>

  <extent>

    <spatial maxx="-123072.53389999999490101" minz="0"
maxz="0" crs="EPSG:3580" dimensions="2" minx="-
170102.13120000000344589" maxy="8454108.23139999993145466"
miny="8395331.84799999929964542"/>

    <temporal>
```

```
      <period>
        <start></start>
        <end></end>
      </period>
    </temporal>
  </extent>
</qgis>
```

of8869_dl_polys

```
<!DOCTYPE qgis PUBLIC 'http://mrcc.com/qgis.dtd' 'SYSTEM'>
<qgis version="3.10.7-A Coruña">

<identifier>of_8869\Data\degraded_lithalsa_polygons\of8869_
dl_polys.shp</identifier>
  <parentidentifier>Morse, P.D., Rudy, A.C.A, 2022.
Distributions of degraded and intact lithalsas, North Slave
region, Northwest Territories; Geological Survey of Canada,
Open File 8869, 1 .zip file.
doi:10.4095/329643</parentidentifier>
  <language>ENG</language>
  <type>dataset</type>
  <title>Degraded Lithalsa Polygons</title>
  <abstract>The main objective of this report is to provide
an inventory of current (intact or degrading) and old
(completely degraded) lithalsas in a representative study
area of the southern North Slave region between Behchoko
and Yellowknife in the Northwest Territories. A lithalsa is
an ice-rich mound of permafrost that causes the soil to
settle downward and water to pond if the ice core thaws
(thermokarst pond). Lithalsas, widespread in this region,
are therefore very sensitive to thawing. This inventory
```

should help to better understand current and future permafrost conditions, and is based directly on the GSC's Open File 7255, which provides an inventory of many lithalsas in the region, as well as on the GSC's Open File 8205, which provides an inventory of thermokarst pond development between 1945 and 2005 in the same study area. Using high-resolution satellite images, we completed the inventory of 475 intact lithalsas in the study area. Then, by combining our field observations of surface geomorphology of degrading lithalsas with recognizable geomorphic patterns in the same satellite imagery, we developed criteria to identify and map them and we developed an inventory of 556 completely degraded lithalsas. The inventories and databases are prepared for assessment of the relations between elevation, surface geology and distribution of lithalsas, and the trajectory of thermokarst development in the region. The inventories included with this report can be used directly in a Geographic Information System (GIS).</abstract>

```
  <keywords vocabulary="gmd:topicCategory">
    <keyword>Environment</keyword>
    <keyword>Geoscientific Information</keyword>
  </keywords>
  <keywords vocabulary="undefined 2">
    <keyword>Lithalsa</keyword>
    <keyword> Thermokarst</keyword>
  </keywords>
  <contact>
    <contactAddress>
      <type>postal</type>
      <address>601 Booth Street</address>
      <city>Ottawa</city>
```

```
      <administrativearea>ON</administrativearea>
      <postalcode>K1A 0E8</postalcode>
      <country>Canada</country>
    </contactAddress>
    <name>Peter Morse</name>
    <organization>Geological Survey of Canada, Natural
Resources Canada</organization>
    <position>Research Scientist</position>
    <voice></voice>
    <fax></fax>
    <email>peter.morse@canada.ca</email>
    <role>owner</role>
  </contact>
  <links>
    <link format="*.zip" mimeType="" type="download" url="
https://doi.org/10.4095/329643" size="" name="GEOSCAN"
description="Open File multi-part report"/>
  </links>
  <fees>None.</fees>
  <rights>© Her Majesty the Queen in Right of Canada, as
represented by the Minister of Natural Resources Canada,
2022.</rights>
  <license>Government of Canada: View the licence agreement
at http://data.gc.ca/eng/open-government-licence-
canada</license>
  <encoding></encoding>
  <crs>
    <spatialrefsys>
```

```
      <wkt>PROJCRS["NAD83 / NWT
Lambert",BASEGEOGCRS["NAD83",DATUM["North American Datum
1983",ELLIPSOID["GRS
1980",6378137,298.257222101,LENGTHUNIT["metre",1]]],PRIMEM[
"Greenwich",0,ANGLEUNIT["degree",0.0174532925199433]],ID["E
PSG",4269]],CONVERSION["Northwest Territories
Lambert",METHOD["Lambert Conic Conformal
(2SP)",ID["EPSG",9802]],PARAMETER["Latitude of false
origin",0,ANGLEUNIT["degree",0.0174532925199433],ID["EPSG",
8821]],PARAMETER["Longitude of false origin",-
112,ANGLEUNIT["degree",0.0174532925199433],ID["EPSG",8822]]
,PARAMETER["Latitude of 1st standard
parallel",62,ANGLEUNIT["degree",0.0174532925199433],ID["EPS
G",8823]],PARAMETER["Latitude of 2nd standard
parallel",70,ANGLEUNIT["degree",0.0174532925199433],ID["EPS
G",8824]],PARAMETER["Easting at false
origin",0,LENGTHUNIT["metre",1],ID["EPSG",8826]],PARAMETER[
"Northing at false
origin",0,LENGTHUNIT["metre",1],ID["EPSG",8827]]],CS[Cartes
ian,2],AXIS["(E)",east,ORDER[1],LENGTHUNIT["metre",1]],AXIS
["(N)",north,ORDER[2],LENGTHUNIT["metre",1]],USAGE[SCOPE["u
nknown"],AREA["Canada - NWT"],BBOX[59.98,-136.46,78.81,-
102]],ID["EPSG",3580]]</wkt>

      <proj4>+proj=lcc +lat_0=0 +lon_0=-112 +lat_1=62
+lat_2=70 +x_0=0 +y_0=0 +ellps=GRS80 +towgs84=0,0,0,0,0,0,0
+units=m +no_defs</proj4>

      <srsid>1538</srsid>

      <srid>3580</srid>

      <authid>EPSG:3580</authid>

      <description>NAD83 / NWT Lambert</description>

      <projectionacronym>lcc</projectionacronym>

      <ellipsoidacronym>EPSG:7019</ellipsoidacronym>

      <geographicflag>false</geographicflag>

    </spatialrefsys>

  </crs>
```

```
  <extent>
    <spatial maxx="-123072.53389999999490101" minz="0"
maxz="0" crs="EPSG:3580" dimensions="2" minx="-
170102.13120000000344589" maxy="8454108.23139999993145466"
miny="8395331.84799999929964542"/>
    <temporal>
      <period>
        <start></start>
        <end></end>
      </period>
    </temporal>
  </extent>
</qgis>
```

of8869_tp_polys

```
<!DOCTYPE qgis PUBLIC 'http://mrcc.com/qgis.dtd' 'SYSTEM'>
<qgis version="3.10.7-A Coruña">

<identifier>of_8869\Data\thermokarst_polygons\of8869_tp_pol
ys.shp</identifier>
  <parentidentifier>Morse, P.D., Rudy, A.C.A, 2022.
Distributions of degraded and intact lithalsas, North Slave
region, Northwest Territories; Geological Survey of Canada,
Open File 8869, 1 .zip file.
doi:10.4095/329643</parentidentifier>
  <language>ENG</language>
  <type>dataset</type>
  <title>Thermokarst Polygons</title>
```

<abstract> The main objective of this report is to provide an inventory of current (intact or degrading) and old (completely degraded) lithalsas in a representative study area of the southern North Slave region between Behchoko and Yellowknife in the Northwest Territories. A lithalsa is an ice-rich mound of permafrost that causes the soil to settle downward and water to pond if the ice core thaws (thermokarst pond). Lithalsas, widespread in this region, are therefore very sensitive to thawing. This inventory should help to better understand current and future permafrost conditions, and is based directly on the GSC's Open File 7255, which provides an inventory of many lithalsas in the region, as well as on the GSC's Open File 8205, which provides an inventory of thermokarst pond development between 1945 and 2005 in the same study area. Using high-resolution satellite images, we completed the inventory of 475 intact lithalsas in the study area. Then, by combining our field observations of surface geomorphology of degrading lithalsas with recognizable geomorphic patterns in the same satellite imagery, we developed criteria to identify and map them and we developed an inventory of 556 completely degraded lithalsas. The inventories and databases are prepared for assessment of the relations between elevation, surface geology and distribution of lithalsas, and the trajectory of thermokarst development in the region. The inventories included with this report can be used directly in a Geographic Information System (GIS).</abstract>

<keywords vocabulary="gmd:topicCategory">

<keyword>Environment</keyword>

<keyword>Geoscientific Information</keyword>

</keywords>

<keywords vocabulary="undefined 2">

<keyword>Lithalsa</keyword>

<keyword> Thermokarst</keyword>

</keywords>

```
  <contact>
    <contactAddress>
      <type>postal</type>
      <address>601 Booth Street</address>
      <city>Ottawa</city>
      <administrativearea>ON</administrativearea>
      <postalcode>K1A 0E8</postalcode>
      <country>Canada</country>
    </contactAddress>
    <name>Peter Morse</name>
    <organization>Geological Survey of Canada, Natural
Resources Canada</organization>
    <position>Research Scientist</position>
    <voice></voice>
    <fax></fax>
    <email>peter.morse@canada.ca</email>
    <role>owner</role>
  </contact>
  <links>
    <link format="*.zip" mimeType="" type="download" url="
https://doi.org/10.4095/329643" size="" name="GEOSCAN"
description="Open File multi-part report"/>
  </links>
  <fees>None.</fees>
  <rights>© Her Majesty the Queen in Right of Canada, as
represented by the Minister of Natural Resources Canada,
2022</rights>
```

```
  <license>Government of Canada: View the licence agreement
at http://data.gc.ca/eng/open-government-licence-
canada</license>

  <encoding></encoding>

  <crs>

    <spatialrefsys>

      <wkt>PROJCRS["NAD83 / NWT
Lambert",BASEGEOGCRS["NAD83",DATUM["North American Datum
1983",ELLIPSOID["GRS
1980",6378137,298.257222101,LENGTHUNIT["metre",1]]],PRIMEM[
"Greenwich",0,ANGLEUNIT["degree",0.0174532925199433]],ID["E
PSG",4269]],CONVERSION["Northwest Territories
Lambert",METHOD["Lambert Conic Conformal
(2SP)",ID["EPSG",9802]],PARAMETER["Latitude of false
origin",0,ANGLEUNIT["degree",0.0174532925199433],ID["EPSG",
8821]],PARAMETER["Longitude of false origin",-
112,ANGLEUNIT["degree",0.0174532925199433],ID["EPSG",8822]]
,PARAMETER["Latitude of 1st standard
parallel",62,ANGLEUNIT["degree",0.0174532925199433],ID["EPS
G",8823]],PARAMETER["Latitude of 2nd standard
parallel",70,ANGLEUNIT["degree",0.0174532925199433],ID["EPS
G",8824]],PARAMETER["Easting at false
origin",0,LENGTHUNIT["metre",1],ID["EPSG",8826]],PARAMETER[
"Northing at false
origin",0,LENGTHUNIT["metre",1],ID["EPSG",8827]]],CS[Cartes
ian,2],AXIS["(E)",east,ORDER[1],LENGTHUNIT["metre",1]],AXIS
["(N)",north,ORDER[2],LENGTHUNIT["metre",1]],USAGE[SCOPE["u
nknown"],AREA["Canada - NWT"],BBOX[59.98,-136.46,78.81,-
102]],ID["EPSG",3580]]</wkt>

      <proj4>+proj=lcc +lat_0=0 +lon_0=-112 +lat_1=62
+lat_2=70 +x_0=0 +y_0=0 +ellps=GRS80 +towgs84=0,0,0,0,0,0,0
+units=m +no_defs</proj4>

      <srsid>1538</srsid>

      <srid>3580</srid>

      <authid>EPSG:3580</authid>
```

```
      <description>NAD83 / NWT Lambert</description>
      <projectionacronym>lcc</projectionacronym>
      <ellipsoidacronym>EPSG:7019</ellipsoidacronym>
      <geographicflag>false</geographicflag>
    </spatialrefsys>
  </crs>
  <extent>
    <spatial maxx="-123072.53389999999490101" minz="0"
maxz="0" crs="EPSG:3580" dimensions="2" minx="-
170102.13120000000344589" maxy="8454108.23139999993145466"
miny="8395331.84799999929964542"/>
    <temporal>
      <period>
        <start></start>
        <end></end>
      </period>
    </temporal>
  </extent>
</qgis>
```